Check for updates

JGR Atmospheres

RESEARCH ARTICLE
10.1029/2021JD035002

Exploring the Effects of Rooftop Mitigation Strategies on Urban Temperatures and Energy Consumption

A. Zonato[1], A. Martilli[2], E. Gutierrez[3], F. Chen[4], C. He[4], M. Barlage[4], D. Zardi[1], and L. Giovannini[1]

[1]Atmospheric Physics Group, Department of Civil, Environmental and Mechanical Engineering, University of Trento, Trento, Italy, [2]Center for Energy, Environment and Technology (CIEMAT), Madrid, Spain, [3]Department of Mechanical Engineering, The City College of New York, New York, NY, USA, [4]National Center for Atmospheric Research, Boulder, CO, USA

Key Points:

- New parameterizations of rooftop mitigations strategies are developed and implemented into the Weather Research and Forecasting (WRF) model
- The new implementations include green roofs and photovoltaic panels, coupled with the BEP + BEM urban canopy models
- Sensitivity tests are conducted in order to evaluate the effect of RMSs on near-surface air temperature and energy consumption

Correspondence to:
A. Zonato,
andrea.zonato@unitn.it

Citation:
Zonato, A., Martilli, A., Gutierrez, E., Chen, F., He, C., Barlage, M., et al. (2021). Exploring the effects of rooftop mitigation strategies on urban temperatures and energy consumption. *Journal of Geophysical Research: Atmospheres*, *126*, e2021JD035002. https://doi.org/10.1029/2021JD035002

Received 1 APR 2021
Accepted 9 OCT 2021

Author Contributions:
Conceptualization: A. Zonato, L. Giovannini
Data curation: A. Zonato
Formal analysis: A. Zonato
Funding acquisition: F. Chen, M. Barlage, D. Zardi, L. Giovannini
Investigation: A. Martilli
Methodology: A. Zonato, A. Martilli, L. Giovannini
Project Administration: F. Chen, M. Barlage, D. Zardi, L. Giovannini
Software: A. Zonato, A. Martilli, E. Gutierrez, C. He
Supervision: A. Martilli, F. Chen, M. Barlage, D. Zardi, L. Giovannini
Validation: A. Zonato
Writing – original draft: A. Zonato, L. Giovannini

© 2021. The Authors.
This is an open access article under the terms of the Creative Commons Attribution License, which permits use, distribution and reproduction in any medium, provided the original work is properly cited.

Abstract This paper describes and evaluates physical parameterizations accounting for the effect of rooftop mitigation strategies (RMSs) on the urban environment, in the context of the mesoscale model Weather Research and Forecasting (WRF). Through the new implementation, the sensitivity of near-surface air temperature and building energy consumption to different RMSs is evaluated by means of numerical simulations in idealized urban areas, for typical summer and winter conditions. Rooftop mitigation strategies considered include cool roofs, green roofs, and rooftop photovoltaic panels. The reference case simulations are performed assuming buildings made by bricks, with roof composed of clay tiles. Results indicate that near-surface air temperature is reduced by cool and green roofs during summer: cool roofs are the most efficient in decreasing air temperature, followed by irrigated green roofs. Photovoltaic panels, instead, induce a temperature increase during daytime and a small decrease during nighttime. Cool roofs reveal to be the most efficient strategy in reducing the energy consumption by air conditioning systems. During wintertime, green roofs maintain a higher near-surface air temperature than clay tile roofs and largely decrease energy consumption. Even PVPs increase air temperature, as in the summer case. On the other hand, cool roofs reduce near-surface air temperature during daytime, inducing an increase in energy consumption. The results presented here show that the parameterization schemes implemented in the WRF model can be a valuable tool to evaluate the effects of mitigation strategies in the urban environment.

Plain Language Summary The increasing number and duration of heatwaves is increasing the heat stress for people living in the cities, and largely increase the use of energy resources. To face this problem, the deployment of rooftop mitigation strategies (RMSs) such as cool roofs, green roofs, and rooftop photovoltaic panels is starting to be adopted worldwide, with the aim of improving thermal comfort for citizens and diminishing the energy demand for heating/cooling of buildings. This article presents the implementation of new numerical schemes, to consider the effect of the above-mentioned roof mitigation strategies on the urban environment, incorporated in the Weather Research and Forecasting (WRF) mesoscale numerical weather prediction model. Different urban configurations have been investigated, varying the height of the buildings and the distance between them, in order to cover a large spectrum of possible cities. Results show that all the rooftop technologies tested in this work decrease air temperature and energy consumption during summer. The effect of RMSs increases with decreasing building height and with increasing building packing density. Results point out that advanced parameterization schemes are needed to simulate the feedback between buildings and the atmosphere, which can be used by urban planners as decision supporting tools to improve the sustainability of urban areas.

1. Introduction

It is well known that rooftop technologies, such as cool roofs (CRs), green roofs (GRs), or rooftop photovoltaic panels (RPVPs) can significantly modify fluxes of energy and momentum in the urban canopy layer (Santamouris, 2014). Their deployment is nowadays largely adopted worldwide, with the aim of improving thermal comfort for citizens and diminishing the energy demand for heating/cooling of buildings (Lai et al., 2019). Therefore, a better understanding of the physical mechanisms driving the

Writing – review & editing: A. Zonato, A. Martilli, D. Zardi, L. Giovannini

modifications induced by rooftop mitigation strategies (RMSs) is desirable, for quantifying their effects on the urban environment, for a wide range of urban structures, and under different climatic conditions. A better comprehension of these processes is receiving increasing attention from planners and policy-makers, especially under growing urbanization and climate change (Chapman et al., 2017). In particular, the increasing number and duration of heatwaves interact nonlinearly with the well-known urban heat island phenomenon (Li & Bou-Zeid, 2013), resulting in extremely high heat stress for citizens and in increased use of energy resources. On the other hand, cold winters present the same features of heatwaves in terms of thermal discomfort and energy demand (Yang et al., 2014), despite cities remain warmer than the surrounding environment. The above-mentioned RMSs have been widely proposed in the literature in recent years, and their effect has been investigated in different specific case studies. While all RMSs reduce the sensible heat release by roofs (and consequently the heat stored into the building materials), acting on the roof surface energy budget, the mechanisms for GRs, CRs, and RPVPs are different. GRs redirect available energy to latent heat at the expense of sensible heat, increasing the evapotranspiration through the vegetation on the rooftop. On the other hand, CRs increase the reflection of the incoming solar radiation by increasing the roof albedo and preventing heat storage within roof materials. Finally, PVPs act as screens for the underlying roof, converting part of the incoming solar radiation into electricity. Several studies quantify the impact of RMSs at the building scale, through field campaigns or numerical simulations (see e.g., Kolokotroni et al., 2013 for CRs, De Munck et al., 2013 for GRs, and Dominguez et al., 2011 for PVPs). However, results cannot be simply upscaled to evaluate mitigation effects at the city scale, because the impact of RMSs depends on urban geometry, thermal properties of the building materials, and climatic conditions, so a different approach is needed. To this purpose, some recent studies employed mesoscale meteorological models to investigate the city-wide impact of RMSs, adopting urban parameterizations with various levels of complexity. For example, Li et al. (2014) evaluated the city-scale mitigation effect of CRs and GRs over the Baltimore-Washington metropolitan area, using the Weather Research and Forecasting (WRF) model coupled with the Princeton Urban Canopy Model, detecting improvements in terms of air temperature during a heatwave period of the same order of magnitude for the two roof technologies. Yang et al. (2014) incorporated the effect of green roofs in the single-layer urban canopy model Noah/SLUCM (Kusaka et al., 2001) and tested it for several megacities, while De Munck et al. (2018) used the Town Energy Balance model (TEB, Masson, 2000), to evaluate the impact of various urban greening scenarios on thermal comfort and energy and water consumption for the city of Paris. For the same city, Masson et al. (2014) demonstrated that PVP arrays can reduce the near-surface air temperature, especially during nighttime. Finally, Salamanca et al. (2016) tested a novel PVP parameterization, coupled with the multilayer urban canopy scheme BEP + BEM (Martilli et al., 2002; Salamanca et al., 2010) for the cities of Phoenix and Tucson, detecting a decrease of both near-surface temperature and energy demand for air conditioning systems (ACSs).

In general, all the above-mentioned studies proposed novel physically based RMS parameterization schemes, which modify the roof surface energy budget, demonstrating a city-wide decrease in air temperature during summer climatic conditions. However, these studies generally lack in generalization, since every RMS parameterization scheme is applied for specific cities under unique climatic conditions. Hence, it is not possible to identify the dependence of the impact of RMSs on urban geometry or atmospheric forcing. Moreover, despite RMSs are worldwide employed to improve thermal conditions in the urban environment during summertime, it is important to evaluate the city-scale effect induced by RMSs also during winter, with the aim of detecting possible reductions in temperatures that may increase thermal discomfort and energy demand for heating systems.

Accordingly, the present study offers a systematic evaluation of the impact of the three above-mentioned RMSs (CRs, GRs, and RPVPs) on both near-surface air temperature and building energy consumption (EC), for a wide range of idealized urban configurations and for two different climatic conditions. To this purpose, GR and RPVP parameterizations have been incorporated in the BEP + BEM urban canopy scheme, in the context of the WRF mesoscale meteorological model (v4.1.2, Skamarock et al., 2019). The modeling system adopted in the present study (WRF coupled with BEP + BEM) has been evaluated through the comparison against measurements in several cities, proving to be a suitable tool to reproduce meteorological conditions and EC in urban areas (e.g., Giovannini et al., 2014; Salamanca et al., 2018).

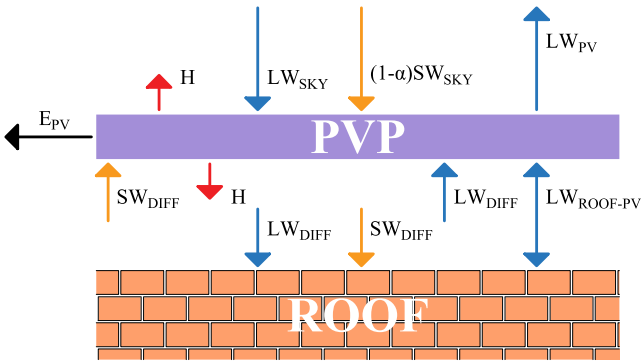

Figure 1. Photovoltaic panel design, with a schematic representation of the energy exchanges with the underlying roof and the environment (SW_{DIFF} e LW_{DIFF}).

The paper is organized as follows: Section 2 describes the schemes adopted to calculate the surface energy budget of RPVPs and GRs, while Section 3 presents the set-up of the idealized simulations and the methods adopted to conduct the sensitivity analysis. Simulations results are discussed in Section 4, focusing on the comparison between simulations in idealized urban areas composed of buildings with clay tile roofs and with the implementation of the RMSs for different urban configurations and climatic conditions. Finally, results are summarized and discussed in Section 5.

2. The Rooftop Mitigation Strategies Schemes

2.1. Rooftop Photovoltaic Panels Parameterization

The parameterization developed in this work in view of taking into account the effects of RPVPs within BEP-BEM assumes the photovoltaic arrays to be parallel and detached from roofs and composed of a single layer. The time derivative of PVP temperature (T_{PV} hereafter) reads (Figure 1):

$$C_{\text{module}} \frac{\partial T_{PV}}{\partial t} = (1-\alpha_{PV})\, SW^{\downarrow}_{\text{sky}} + \varepsilon^{U}_{PV} LW^{\downarrow}_{\text{sky}} - LW^{\uparrow}_{PV} + LW^{\updownarrow}_{roof-PV} \tag{1}$$

$$- \; E_{PV} - H^{\uparrow} - H^{\downarrow} \tag{2}$$

$$+(1-\text{VF})\left[(1-\alpha_{PV})\, SW_{\text{DIFF}} + LW^{\downarrow}_{\text{sky}}\right] \tag{3}$$

with (all terms in W m^{-2}):

- $C_{\text{module}} = 5.72$ MJK^{-1} m^{-2} is the equivalent heat capacity per unit area, assuming that the PVP is composed of three layers, as in Jones and Underwood (2002): a monocrystalline silicon PV cell, a polyester trilaminate and a glass face, with a total depth of 6.55 mm. For the values of heat capacity, depth, and density for each layer, refer to Jones and Underwood (2002)
- $(1-\alpha_{PV})SW^{\downarrow}_{\text{sky}}$: net shortwave radiation gained by the upward surface of the PVP, assuming an albedo $\alpha_{PV} = 0.11$
- $\varepsilon^{U}_{PV} LW^{\downarrow}_{\text{sky}}$: incoming longwave radiation at the upper surface of the PVP, where $\varepsilon^{U}_{PV} = 0.79$ is the emissivity of the glass face
- $LW^{\uparrow}_{PV} = \varepsilon^{U}_{PV}\sigma T^{4}_{PV}$: upward longwave radiation emitted by the PVP
- $LW^{\updownarrow}_{\text{roof}-PV} = \text{VF}\,\frac{1}{\frac{1-\varepsilon^{D}_{PV}}{\varepsilon^{D}_{PV}} + \frac{1-\varepsilon_{\text{roof}}}{\varepsilon_{\text{roof}}}}\sigma\left(T^{4}_{PV} - T^{4}_{\text{roof}}\right)$: longwave radiation exchanged between the monocrystalline silicon downward face of the PVP ($\varepsilon^{D}_{PV} = 0.95$) and the upward face of the roof. The radiation fluxes coming from the PVP and from the roof are considered together in order to take into account the multiple reflections between the two surfaces. VF is the view factor between the downward face of the PVP and the roof. Assuming a 10 m × 10 m PVP (covering completely the roof, with a clearance of 0.3 m from the underlying surface, VF = 0.06)
- $E_{PV} = \eta_{PV} SW^{\downarrow}_{\text{sky}} \min\left[1, 1-0.005\,(T_{PV}-298.15)\right]$: energy production by the PVP. It takes into account that the efficiency of PVPs decreases at temperatures higher than 25°C; η_{PV} is the conversion efficiency of the PVP, that is, the fraction of shortwave radiation converted into electricity. Efficiency varies from 7% for quantum dot cells to 44% for multijunction cells used in research applications (NREL, 2020). In this work, since the most common arrays used for rooftop are monocrystalline and polycrystalline silicon PVPs, we use an efficiency $\eta_{PV} = 0.19$
- $H^{\uparrow} + H^{\downarrow} = \left(h^{\uparrow} + h^{\downarrow}\right)(T_{PV} - T_{\text{air}})$: the sensible heat fluxes at the upward and downward faces of the PVP. The formulation for $h = \sqrt{h_c^2 + a|V|^b}$ depends on empirical fits and is adopted from the EnergyPlus model (US Department of Energy, 2010), which has been validated against measurements (Scherba et al., 2011). h_c depends on the material of the surface (glass, in this case), on whether the surface faces upward or downward, and on the sign of the difference between surface and air temperature. The

absolute value of wind speed is taken at the first level of WRF above the roofs and it is supposed to be the same for the upward and downward face

- $(1 - \mathrm{VF})\left[(1-\alpha_{PV})SW_{\mathrm{DIFF}} + LW^{\downarrow}_{\mathrm{sky}}\right]$: diffuse shortwave and longwave isotropic radiations reaching the downward PV surface. $LW^{\downarrow}_{\mathrm{sky}}$ is the incoming longwave radiation, while SW_{DIFF} is the diffuse shortwave radiation. The same amount of diffuse shortwave and longwave radiation reaches also the roof below the PVP.

Differently from Masson et al. (2014) and Salamanca et al. (2016), which parameterized T_{PV} through its dependence on shortwave solar radiation, here we directly solve numerically Equation 1, in a way similar to Jones and Underwood (2002), to get a PVP temperature that depends on all the involved contributions. Once T_{PV} is calculated, the value of the outgoing heat flux is updated and passed to the multilayer urban scheme.

2.2. The Green Roofs Parameterization

The land-surface scheme for GRs has been developed based on de Munck et al. (2013) and Gutierrez (2015). It calculates energy and water budgets, taking into account incoming net radiation, water input from precipitation and irrigation, evapotranspiration from vegetation, heat exchange with the atmosphere, and diffusion of energy and moisture throughout the soil. The model is one-dimensional, that is, horizontal transport and subsurface flows are neglected.

A GR consists of 10 layers with a total depth of ~0.3 m (Figure 2). Five levels (0.08 m of total thickness) represent the organic matter substrate where vegetation grows. Vegetation roots reach the bottom of the substrate, and vegetation is assumed to intercept all the incoming radiation from the atmosphere. One layer represents the drainage layer (0.05 m), where surplus water is removed. Finally, four levels describe the insulation layer, composed of a waterproofing membrane (0.003 m), an insulating sheet (0.06 m), a further waterproofing membrane (0.003 m), and finally a layer for insulating the structural roof (0.1 m).

2.2.1. Hydrology for Green Roofs

The latent heat flux LE is modeled considering only evaporation from soil moisture and transpiration through leaves of the water absorbed by roots in the layers composing the substrate:

$$LE = \frac{\rho_a L\,(q_{surf,S} - q_a)}{R_a + R_S} \tag{4}$$

where ρ_a is the air density, L the latent heat of vaporization, $(q_{surf,S} - q_a)$ the difference between the saturated soil specific humidity and the actual air humidity around the plants (de Munck et al., 2013), R_a the aerodynamic resistance (Louis, 1979) and R_S the stomatal resistance. The latter depends on the atmospheric state, water availability, and vegetation features, and it is written as:

$$R_S = \frac{R_{S_{\min}}}{LAI\; F_1 F_2 F_3 F_4} \tag{5}$$

where $R_{S_{\min}}$ is the minimum stomatal resistance of the vegetation, while LAI is the leaf area index. F_1 describes the effect of photosynthetic radiation, F_2 the hydrological features, F_3 and F_4 the effect on evapotranspiration of temperature and humidity, respectively (see Jacquemin & Noilhan, 1990 for more details). The Richards' equation (Short et al., 1995) is used to represent the one-dimensional transport of soil moisture (Θ) throughout the soil:

$$\frac{\partial \Theta}{\partial t} = \frac{\partial}{\partial z}\left(D\frac{\partial \Theta}{\partial z} + K\right) + F_\Theta \tag{6}$$

where D and K are, respectively, soil water diffusivity and hydraulic conductivity calculated as:

$$K = K_S\left(\frac{\Theta}{\Theta_S}\right)^{2b+3} \tag{7}$$

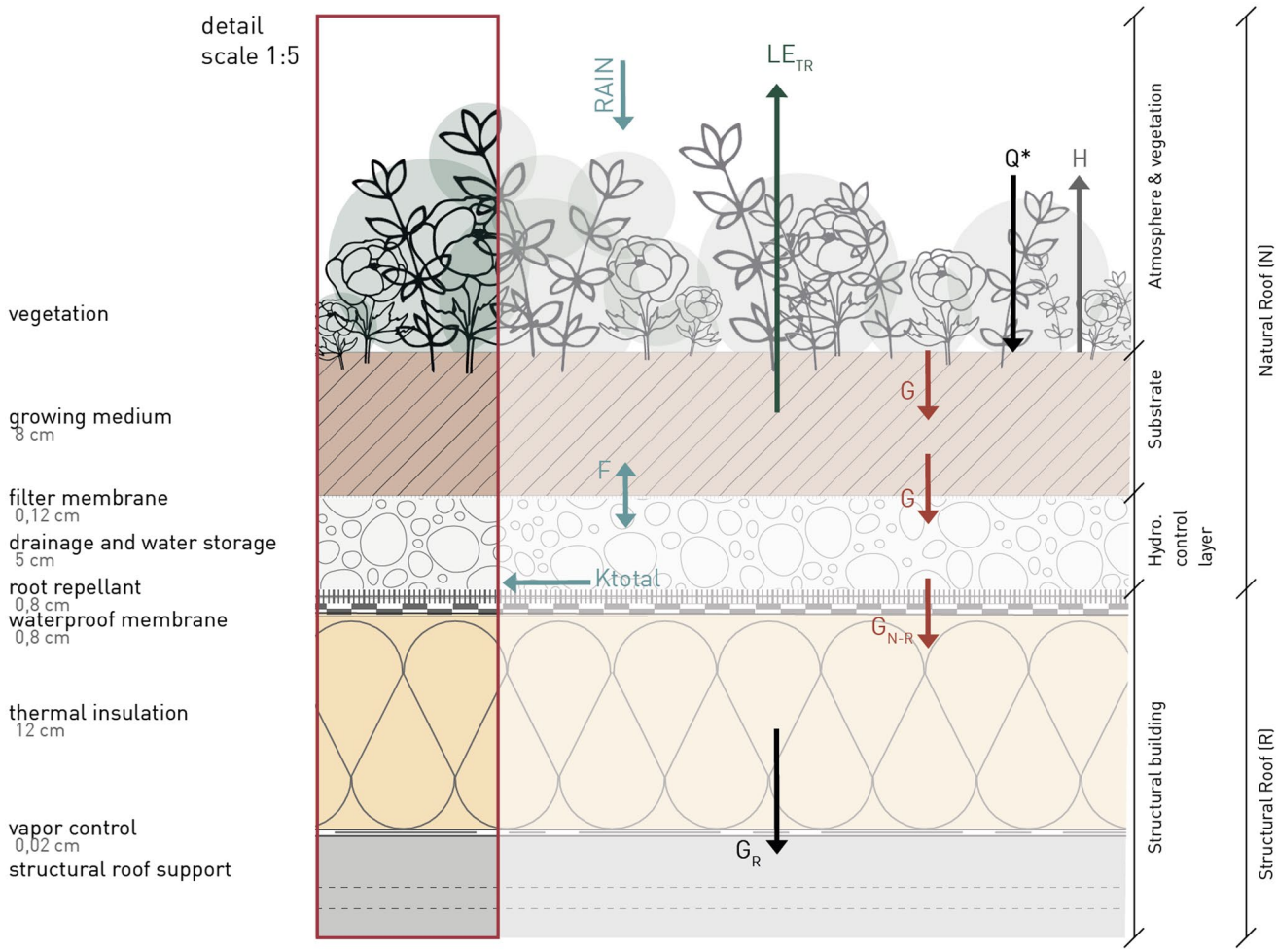

Figure 2. Green roof design. Arrows refer to the sensible/latent heat exchange between the different layers and the atmosphere.

$$D = \frac{-bK_S\Psi_s}{\Theta}\left(\frac{\Theta}{\Theta_S}\right)^{b+3} \tag{8}$$

$\Psi = \Psi_s\left(\frac{\Theta_S}{\Theta}\right)^b$ is the moisture potential, $b = 3.9$ is an empirical coefficient of water retention of organic matter, while all the terms with the subscript "S" refer to the soil in saturation conditions. F_Θ considers all source and sink terms. For the uppermost layer $F_\Theta = Ir + P - E$, where Ir is the irrigation, P the precipitation rate, and E the evapotranspiration. For the drainage layer, just under the substrate, $F_\Theta = -K$ represents the surplus rain drained, if in excess.

2.2.2. Thermodynamics for Green Roofs

The heat transfer between GRs layers is calculated using the Fourier diffusion equation for soil temperature (T):

$$\frac{\partial T}{\partial t} = \frac{\partial}{\partial z}\left(\lambda\frac{\partial T}{\partial z}\right) + F_T \tag{9}$$

where F_T represents source and sink terms. For the uppermost layer F_T is calculated from the surface energy balance:

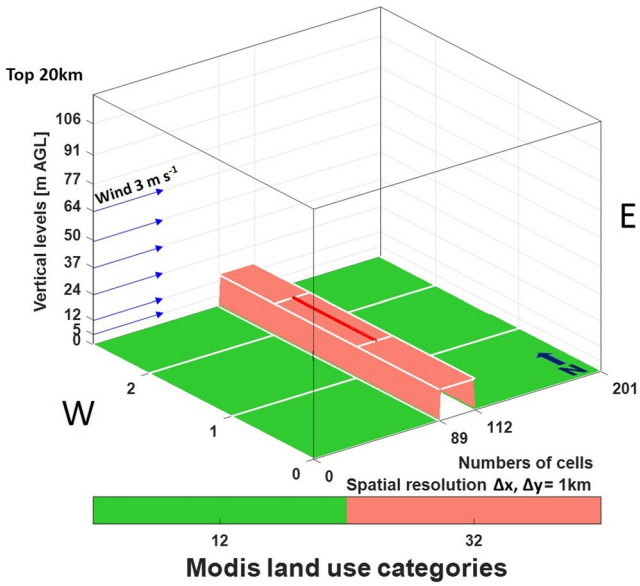

Figure 3. Schematic representation of the domain used for the idealized simulations. The red line represents the cell chosen to analyze the numerical results, from Pappaccogli et al. (2020).

$$\frac{F_T}{\Delta z \lambda} = H - LE + (1 - \alpha_{GR}) SW^{\downarrow}_{\text{sky}} + LW^{\downarrow}_{\text{sky}} - LW^{\uparrow}_{GR} \tag{10}$$

where α_{GR} is the albedo of the GR, λ the thermal diffusivity of the substrate layers and $LW^{\uparrow}_{GR} = \varepsilon_{GR}\sigma T^4_{GR}$ is the longwave radiation emission of the GR, with $\varepsilon_{GR} = 0.93$ the emissivity of the GR and T_{GR} its surface temperature. For the layer close to the conventional roof, F_T is the heat conduction flux calculated using the temperature gradient between the bottom layer of the natural roof and the uppermost layer of the structural roof, using a weighted average of their thermal diffusivities. The thermal diffusivity for natural roof layers depends on soil moisture:

$$\lambda = \begin{cases} \dfrac{e^{-(log_{10}|\Psi|+2.7)}}{C_S} 4.186 \times 10^7 \ \ if\ log_{10}|\Psi| \le 5.1 \\ \dfrac{4.1\times10^{-5}}{C_S} 4.186 \times 10^7 \ \ if\ log_{10}|\Psi| > 5.1 \end{cases} \tag{11}$$

where $C_S = (1 - \Theta)C_d + \Theta C_w$ is the volumetric specific heat for wet soil, calculated as the weighted average of the volumetric specific heat for dry soil (C_d) and water (C_w).

3. Methodology

3.1. Set-Up of the Idealized Simulations

The set-up of the idealized simulations is similar to the one proposed in Pappaccogli et al. (2020). The effect of different RMSs on air temperature and EC has been evaluated through two-dimensional idealized simulations for various urban geometries and under different meteorological conditions. The idealized simulations, also thanks to their low computational cost, allows investigating a great number of cases, adopting different urban geometries under controlled atmospheric conditions. A total of 168 simulations has been performed for an ideal city situated at a latitude of 45°N. Two different seasons are simulated: a typical summer period (June 21–23, SUM hereafter) and a typical winter period (December 21–23, WIN hereafter), to quantify the effects of rooftop modifications with completely different solar radiation forcing. Simulations consist of a common numerical domain (Figure 3), composed of 200 × 3 grid cells with a horizontal spatial resolution of 1 km and 51 vertical grid cells with a finer resolution close to the ground, with nine cells in the first 110 m. Simulations run with a time step of 10 s, starting at 00:00 LST for 72 hr. The first 24 hr are considered as spin-up period, allowing to reach a quasi-steady diurnal cycle, while the last 48 hr are taken into account for the sensitivity analysis. Initial conditions are specified adopting a potential temperature profile with a positive gradient of 3.5 K km^{-1} and a westerly wind with an intensity of 3 m s^{-1} constant with increasing height. Surface temperature is set to 27°C in SUM and to 4°C in WIN everywhere in the domain. The relative humidity is set to 20% and 50% at the surface for SUM and WIN, respectively, linearly decreasing to 0% at ~5,000 m above ground level.

Regarding physics parameterizations, the Bougeault and Lacarrere (1989) scheme is used as Planetary Boundary Layer (PBL) parameterization, while Noah-MP (Niu et al., 2011) is adopted for land-surface processes. Stamnes et al. (1988) is used for shortwave radiation and the Rapid Radiative Transfer Model (RRTM, Mlawer et al., 1997) for longwave radiation. Horizontal turbulent exchange coefficients are kept constant and equal to 300 m^2 s^{-1}. Finally, microphysics and cumulus schemes are turned off, to avoid the formation of clouds. Periodic lateral boundary conditions are set for all the input variables, in both N-S and W-E directions.

A 23-km wide city is situated in the center of a completely flat domain, while the surrounding rural areas are classified as "cropland," according to the MODIFIED IGBP MODIS NOAH classification in WRF. The width of the city is the same for all the simulations, as well as buildings and urban ground thermal properties. Since this work aims at quantifying the impact of different mitigation strategies on air temperature

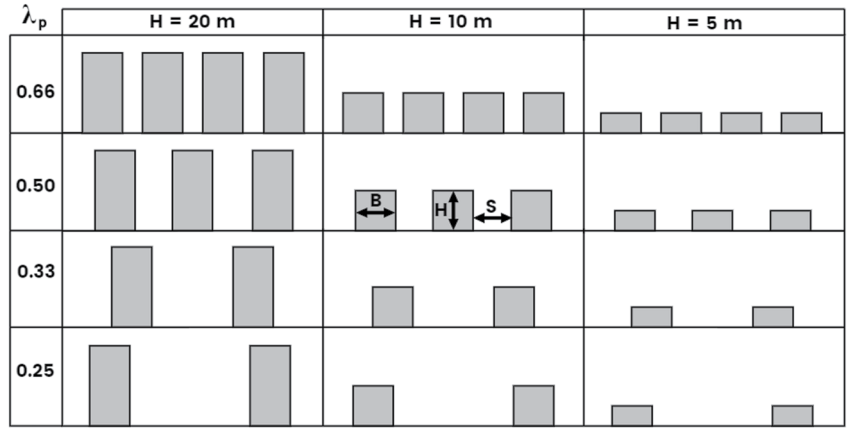

Figure 4. Schematic representation of the 12 different urban configurations for the idealized simulations. *B* is the building width, *S* the street width, *H* the building height, and λ_p the building area to total area ratio.

and EC, several geometrical building features are tested, to consider a large spectrum of possible urban configurations. In Figure 4, the schematic representation of all the scenarios simulated in this work is shown. For all the simulations, the building width B is set to 10 m, and artificial surfaces are supposed to occupy the entire cell, hence the urban fraction is set to 1. The urban geometry in the simulations varies depending on building height, which is set to 5, 10, and 20 m, and building surface to total surface fraction, defined as $\lambda_p = B/(B+S)$, where S is the street width. λ_p varies with the street width, that is set, ranging from scattered to packed configurations, equal to 30, 20, 10, and 5 m, resulting in $\lambda_p = 0.25$, 0.33, 0.50, and 0.66, respectively. This range of λ_p has been identified by Grimmond and Oke (1999) as representative of most of the cities worldwide. Hence, the 12 possible building geometric configurations represent a wide range of Local Climate Zones, from residential areas with low and scattered buildings, to city centers with high and compact buildings. For all the simulations, thermal and physical properties of buildings are kept constant (Table 1). In particular, building walls are assumed to be composed of solid brick, with windows covering 20% of the surface, while roofs are covered with clay tiles. No insulating layers are assumed within roofs and walls. For ground, we adopt thermal parameters of asphalt (values are taken from Oke et al., 2017). SUM and WIN differ with respect to the indoor target temperature. It is set to 20°C for WIN and to 25°C for SUM, according to the directive UNI/TS 11300-1 (Pappaccogli et al., 2018; UNI/TS 11300-1, 2014). Internal temperature fluctuations of ±2°C are permitted, and it is prescribed that the heating/cooling system is on during the whole time of the simulations. For WIN a coefficient of performance (COP) of 0.9 is adopted, which represents the average energy efficiency of most heating systems (i.e., gas and fuel-fired boilers, electrical resistance heaters, heat pumps, etc., Martilli, 2014), while for SUM it is set to 3.5, representing the typical coefficient of performance of ACSs. In order to estimate the energy consumed per person (and to calculate the heat generated by inhabitants), 0.02 person m^{-2} are assumed within buildings, a typical value for European cities (Eurostat, 2018).

Table 1
Thermal and Physical Parameters for the Idealized Simulations

	Roof	Walls	Road
Heat capacity (MJ m^{-3} K^{-1})	1.77	1.37	1.94
Thermal conductivity (W m^{-1} K^{-1})	0.84	0.83	0.75
Albedo	0.30	0.35	0.15
Emissivity	0.90	0.90	0.95
Target temperature for ACs (°C)	25 ± 2 (SUM), 20 ± 2 (WIN)		
Percentage of glass windows	20%		
Persons per area (person m^{-2})	0.02		

3.2. Sensitivity Analysis

In this work, we quantify the effect on near-surface air temperature and EC of the implementation of several RMSs with respect to clay tiles roofs (NORMS), taken as the reference simulation for each urban configuration, for a total of 12 different urban geometries (combination of three building heights and four λ_p). In particular, a total of six RMSs are tested, as here summarized:

1. Cool Roof (CR): for this scenario, the clay tiles roof albedo (Table 1) is replaced with $\alpha = 0.80$
2. Green Roof with grass (GRASS): the roof is supposed to be completely covered with a green roof, as shown in Figure 2. The GR is covered by grass, assuming $LAI = 2$, $\alpha_{gr} = 0.154$, $R_{S_{\min}} = 40$ and initial green roof soil moisture $SM = 0.2\ \mathrm{m^3 m^{-3}}$
3. Green Roof with sedum (SEDUM): same as GRASS, but in this case the GR is covered with sedum, assuming $LAI = 3$, $\alpha_{gr} = 0.3$, and $R_{S_{\min}} = 150$. Sedum is the most frequent vegetation type used for GRs in dry and moderate climates, due to their ability to withstand long periods of heat and water stress by partially closing their stomata during the day (de Munck et al., 2013)
4. Green Roof with grass and irrigation (GRASS + IRRI): same as GRASS, but assuming to irrigate the GR vegetation in the period 01:00–03:00 LST. A total of 25 L $\mathrm{m^{-2}}$ of water per week (as in De Munck et al. (2018)) is set at the surface of the uppermost GR layer
5. Photovoltaic panels (PVP): photovoltaic panels with albedo $\alpha = 0.11$ and efficiency $\eta_{PV} = 0.19$ (typical of monocrystalline silicon cells) are assumed to be superimposed over all the roofs, 0.3 m over them
6. Green Roof with grass and photovoltaic panels (GRASS + PVP): same as GRASS, but with the GR covered with PVPs. PVPs are assumed to be 0.3 m above the green roof

4. Results

In this section, the differences in 2-m air temperature and EC between the simulations implementing the RMSs and NORMS are evaluated. Results are analyzed considering both the full diurnal cycles, to understand when RMSs are more effective, and the average differences over all the simulation period, to evaluate which is the best mitigation strategy and with which urban configuration. Finally, the analysis focuses on temperature and energy budget time series at the roof level, to understand the physics governing each RMS. Results are presented separately for SUM and WIN, to better understand the effects of the RMSs in the two seasons. Since the diurnal cycles of the variables considered here are very similar on the 2 days analyzed, we decided to average both days into a single diurnal cycle, to cancel out random fluctuations and obtain more robust results.

4.1. Summertime

Figure 5 shows the diurnal cycle of 2-m air temperature (left) and EC by air conditioning per person (right) for the central cell representing the idealized city in the NORMS simulations. The solid line represents the mean value of the different simulations, while the variability is shown by the shaded regions. On average, a maximum temperature of ~36°C is reached at 15:00 LST, while the minimum temperature is ~27°C at 05:00 LST. These temperature values are representative of typical climatic conditions during a strong heatwave in an urban area at midlatitudes. Temperature variability between different urban configurations is low during daytime, while it becomes larger during nighttime, because of the strong influence of the urban geometry on UHI intensity during nighttime (Martilli, 2014; Zonato et al., 2020). EC is very low during nighttime when indoor temperature decreases below the target value and ACSs are not needed (for some cases), while it reaches its maximum around 16:00 LST (~2.3 kWh per person), shifted by 1 hr with respect to the 2-m air temperature peak, due to the thermal inertia of the buildings. The variability of EC between different urban configurations is higher during daytime with respect to temperature variability, since EC for each cell does not depend only on external temperature but has a strong dependence also on urban morphology, and in particular on the number of floors in each cell. In fact, buildings with more than one floor exhibit a lower EC per person, since overlaying floors insulate lower floors and reduce heat dispersion in the vertical direction.

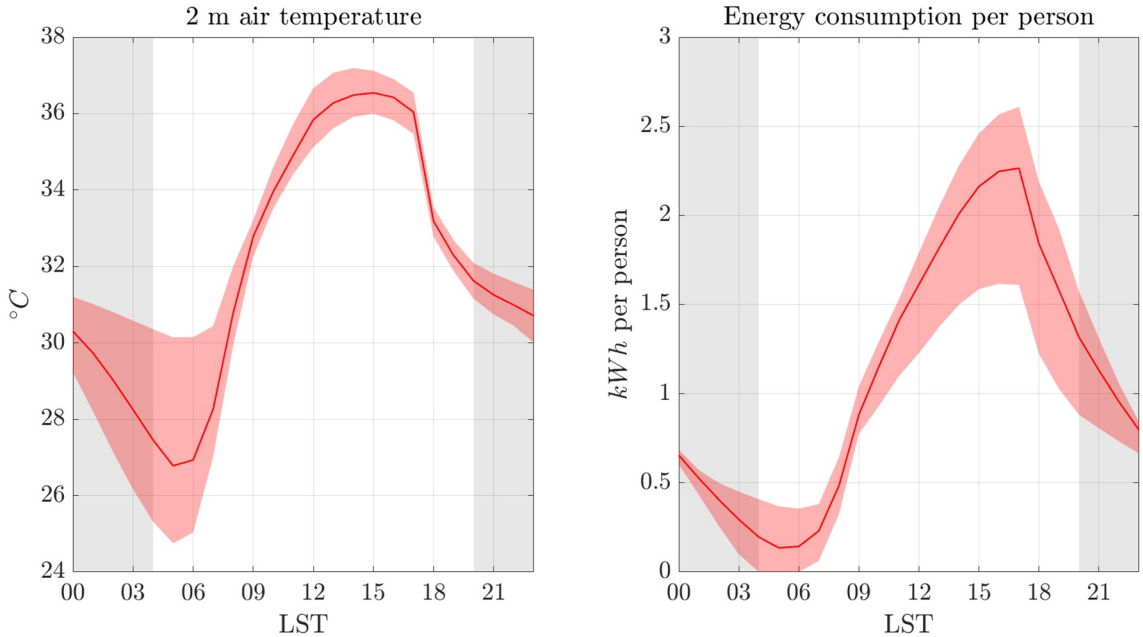

Figure 5. Summertime average air temperature at 2-m AGL (left) and energy consumption per person (right) averaged over a single diurnal cycle for the NORMS simulations (red line). The red shaded regions represent the variability obtained in the simulations with different urban configurations. Shaded background indicates nighttime hours.

4.1.1. Impact on 2-m Air Temperature

Figure 6 shows the time series of 2-m air temperature differences between the NORMS scenario and all the RMSs for all the possible urban configurations. A feature common to CR and GR is a general decrease in temperature for all configurations, with higher differences for lower buildings (the roof surface is closer to the ground, so the effect of the RMSs is more intense) and higher λ_p (the cooling effect increases as a larger ground surface is covered by buildings). For all RMSs, the diurnal cycles in Figure 6 are mainly driven by

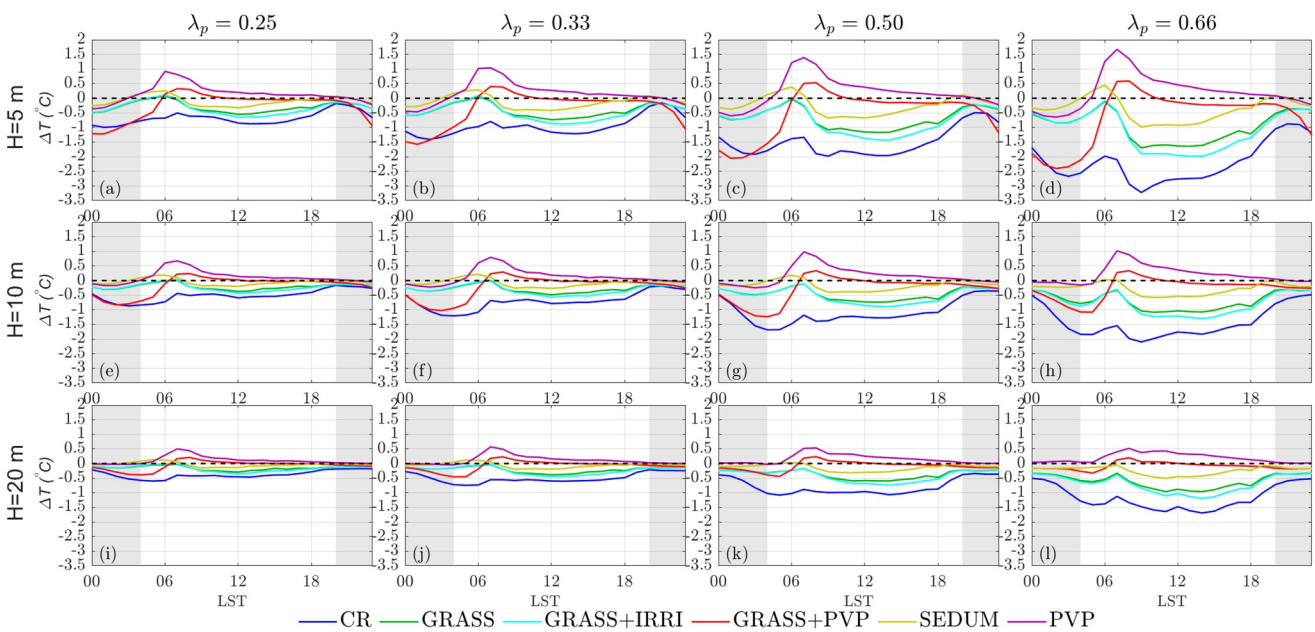

Figure 6. Summertime 2-m air temperature differences between NORMS and each rooftop mitigation strategy, averaged for the central urban cell, and for a single diurnal cycle. Building height is kept constant along the rows, while λ_p along the columns. Shaded background indicates nighttime hours.

radiation: the largest mitigation effect takes place in the central hours of the morning (08:00–10:00 LST) for CRs, when radiation starts to increase and in the central hours of the day (12:00–14:00 LST) for GRs, when less available radiation is converted into sensible heat. A secondary negative peak is present in the central hours of the night for the GR cases, due to the reduced storage of heat within buildings. However, this effect rapidly vanishes around sunrise (05:00–06:00 LST), when small positive differences (i.e., higher temperatures) are present. This is due to the larger temperature gradients between roof surfaces and air, and, as a consequence, higher sensible heat fluxes, as will be shown in Section 4.1.3.

CR presents a nocturnal peak of reduction of air temperature at 03:00 LST. This nocturnal counter intuitive peak is due to the combination of several factors: (a) the reduction of the heat stored in the roofs, and a small release during nighttime, (b) the city-wide reduction of temperature during daytime, which affects also the nighttime period, and (c) the decrease of energy consumption by ACSs (as shown in Figure 8), that consequently reduces the heat emitted by buildings.

PVP and GRASS + PVP cases behave differently with respect to the others RMSs: both show an increase in temperature during daytime, with a sharp peak of ∼1.5°C at 08:00 LST. This is due to the fact that the PVP is thin (6.55 mm), so it presents a smaller thermal inertia than the roof surface. For this reason, air temperature for the PVP cases remains higher during the day, with higher values for packed and low buildings. Moreover, for the configurations with $H = 5$ m, during the night temperature is lower than in NORMS, since the shading effect of the PVP avoids the heat to be stored and then released during nighttime, with differences up to ∼0.5°C. This effect is negligible for higher buildings, which present a smaller influence on near-surface air temperature. GRASS + PVP shows a behavior similar to PVP, even if the presence of the GR mitigates the effect of the PVP for all the diurnal cycles, with a diurnal peak up to ∼0.5°C and a minimum value during nighttime comparable with the CR case. The highest impact during daytime is detected in the $H = 5$ m, $\lambda_p = 0.66$ configuration (panel d), with a maximum reduction of ∼3.3°C at 08:00 LST for CR. It is followed by GRASS + IRRI and GRASS, which reduce the temperature during the peak of solar radiation of ∼2°C and ∼1.7°C, respectively. The difference between these two cases, that is, with and without irrigation, increases as the simulation time advances: indeed, while for GRASS the soil moisture continues to diminish, for GRASS + IRRI the soil moisture is periodically increased by irrigation (not shown). SEDUM and PVP display an average temperature reduction of ∼0.8 °C, with a peak at 13:00 LST for the latter. Despite SEDUM and GRASS share the same roof design, the different type of vegetation deployed on the roof changes the impact on the surface energy balance. Grass is more efficient with respect to sedum in converting solar radiation to latent heat flux, resulting in a lower outgoing sensible heat flux.

In order to quantify the average effect of the different RMSs varying the urban configuration, 2-m air temperature differences are averaged for all the period of simulation and compared for each building height (Figure 7). As said before, CR is the most effective RMS, with an average reduction of ∼2.2°C. The negative temperature differences induced by GRs and CRs display a quasi linear increase with increasing λ_p, with increasing negative slope as the efficiency of the RMS increases. For example, for 5-m high buildings the difference between CR and SEDUM is of ∼0.4°C for $\lambda_p = 0.25$ and of ∼1.7°C for $\lambda_p = 0.66$. With increasing building height the effect of the RMSs diminishes, and so does also the difference between the slopes. PVP is the only RMS that shows average increases of air temperature, with slightly increasing differences as λ_p increases. However, the average effect of PVP is low, and no particular trends have been detected varying the building height.

While the effects of the RMSs are linear with respect to λ_p, temperature reduction is not linear with decreasing building height: if λ_p is kept constant, the difference in temperature reduction between $H = 5$ m and $H = 10$ m is higher compared to that observed between $H = 10$ m and $H = 20$. Again, apart from PVP, SEDUM is the least efficient strategy in mitigating 2-m air temperature, since this type of vegetation converts less radiation into latent heat flux with respect to all the simulations with grass. Focusing on GRASS and GRASS + IRRI, it is possible to notice that GRASS + IRRI is slightly more efficient in reducing 2-m air temperature: assuming to irrigate the GR during nighttime, the latent heat flux during daytime will be higher with respect to the case without irrigation, resulting in a reduced sensible heat flux release. Finally, GRASS + PV shows a net temperature decrease for $H = 5$ m, even higher than in SEDUM. Increasing the building height, the effects induced by GRASS + PVP disappear, being almost null for $H = 20$ m.

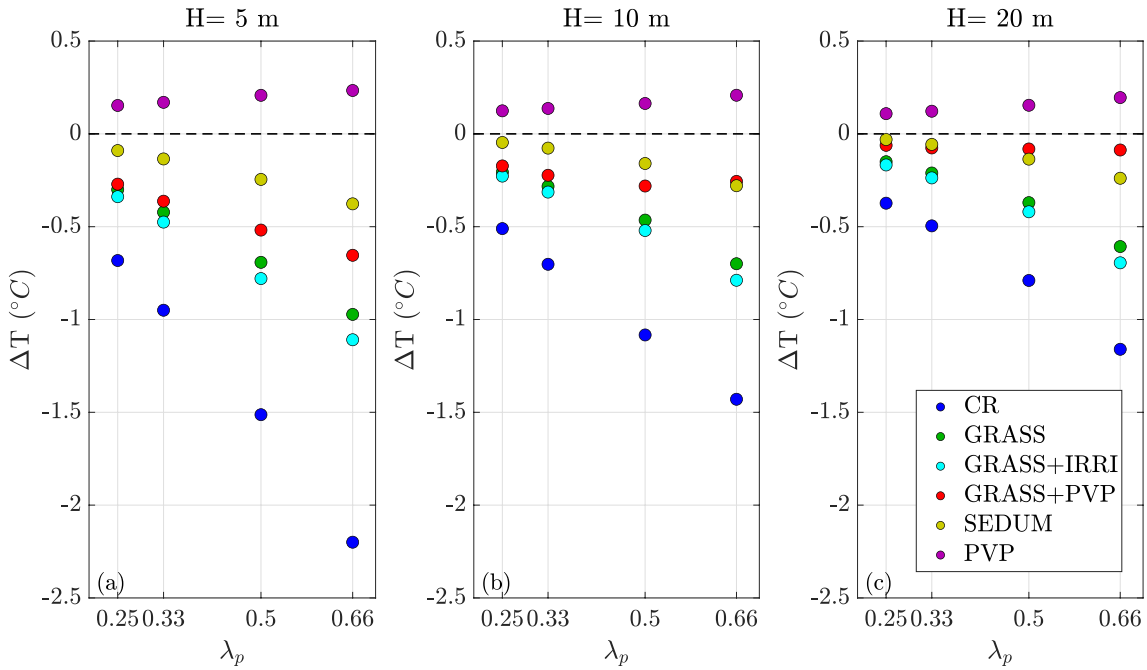

Figure 7. Summertime 2-m air temperature differences for each rooftop mitigation strategy averaged over all the period of simulations, depending on λ_p. The left panel shows 5-m building configurations, central panel 10-m buildings, and right panel 20-m buildings.

4.1.2. Impact on Energy Consumption

Figure 8 shows the time series of the differences in EC per person between NORMS and all the RMSs for all the possible urban configurations. Also in this case, it can be seen that the effect of the RMSs increases with increasing λ_p and with decreasing building height. The impact of RMSs is more significant in the floor close to the roof, therefore a higher reduction of EC is found for low buildings, composed of a single floor, than for higher buildings, where the effect on lower floors is lower. The different RMSs do not affect EC in the same way they affect air temperature: the largest reduction occurs at 15:00 LST for CR, coincident with the EC peak, and at 17:00 LST for simulations with GRs and for PVP. The shift in time of the maximum difference is probably linked to the higher thermal inertia of the insulating waterproof layers composing the GRs, and to the screening effect of the PVPs. All the simulations implementing GRs and CR show a similar maximum reduction in EC, by ~0.8 kWh per person for $H = 5$ m, larger than for PVP (~0.2 kWh per person). However, CR displays a higher EC reduction in the night and in the morning. It is remarkable that, despite different types of vegetation and soil moisture, GR cases show the same reduction in EC. This means that the impact of the insulating waterproof layer, which prevents heat from penetrating into the roof, is more important than the effect of the different surface energy balance, even if a PVP layer is superimposed. If the energy produced by PVPs is neglected in the net computation of EC, the PVP case is the least efficient in diminishing EC: while the screening effect is beneficial during daytime, with a consequent decrease coincident with the peak of EC, during nighttime it prevents the heat to be released by the roof surface through longwave radiation, resulting in an increase of EC. The maximum increase in EC takes place at the same hour as the maximum increase of temperature, around sunrise (Figure 7), due to the cumulative effect of the reduced radiative cooling occurring during nighttime.

In Figure 9, the cumulative difference in EC per person is shown for each RMS, expressed as a percentage with respect to NORMS, for all the period of simulation and for each urban configuration. The decrease in EC becomes linearly larger with growing λ_p for all the RMSs: this linearity is mainly due to the linear decrease of 2-m air temperature, which contributes to diminishing the EC by ACSs. As shown in Figure 8, all the simulations implementing GRs perform similarly in reducing EC, with a cumulative decrease comparable to the CR case. While CR and simulations with GRs can diminish EC up to 30–45% for 5-m buildings, PVP does not reduce EC, due to the compensation of the decrease during daytime and the increase during

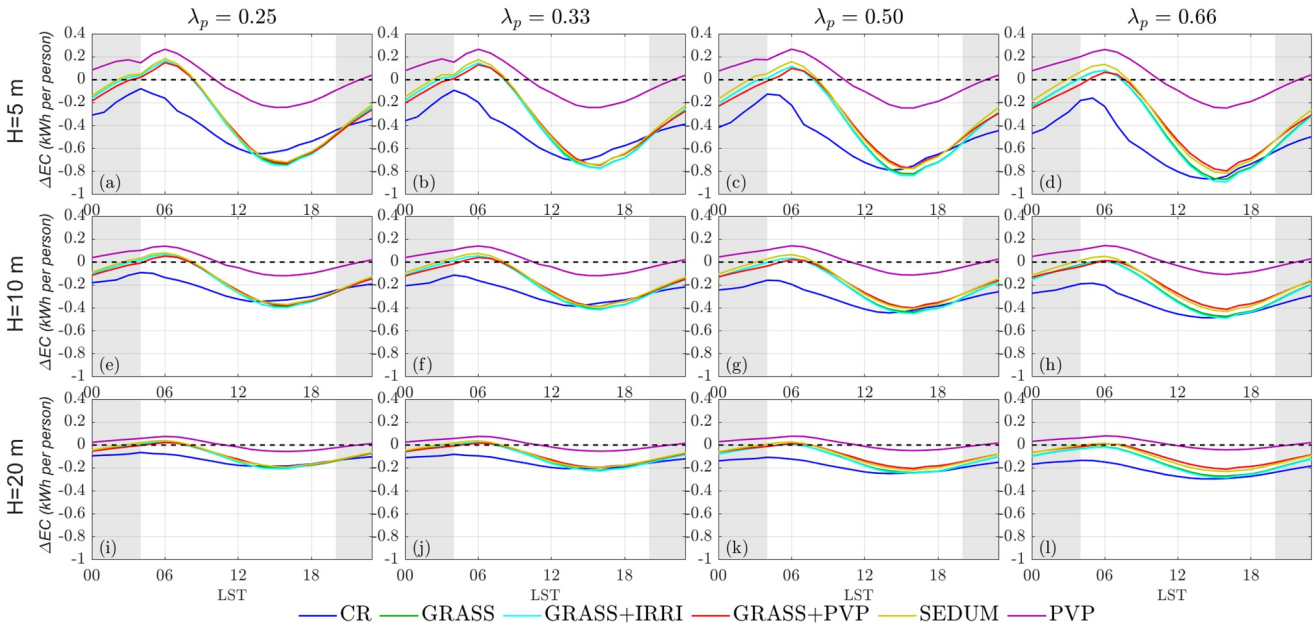

Figure 8. Differences in energy consumption per person between NORMS and each rooftop mitigation strategy averaged for the central urban cell and for a single diurnal cycle during summertime. Building height is kept constant along the rows, while λ_p along the columns. Shaded background indicates nighttime hours.

nighttime. In fact, while CRs prevent 80% of radiation to reach the roof, PVPs reflect only 11% of radiation and convert an additional 19% into electricity. Therefore, radiation entering the surface energy budget is almost four times higher in PVP with respect to CR. Moreover, no additional insulating layers as in the simulations with GRs are implemented in PVP, resulting in a higher heat flux through the roof layers. However, if we assume to instantly use electricity produced by PVPs for the ACSs energy supply, we have a surplus of

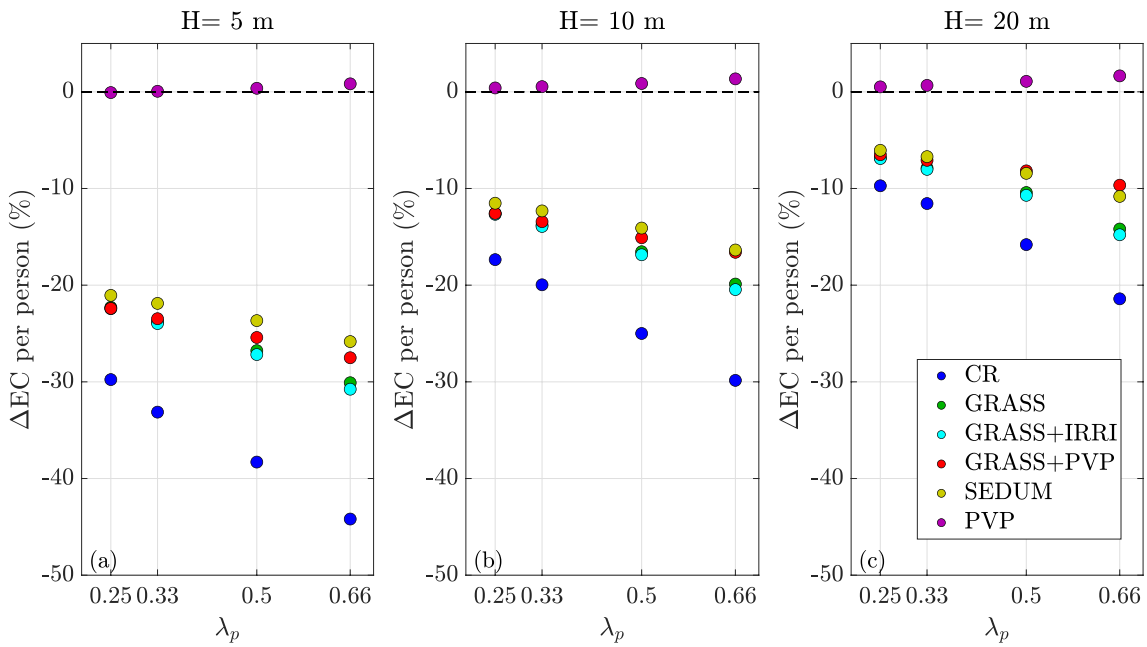

Figure 9. Variation (percentage) in energy consumption per person with respect to the NORMS case, for each rooftop mitigation strategy for all the period of simulation during summertime, depending on λ_p. The left panel shows results for 5-m buildings, the central panel for 10-m buildings and the right panel for 20-m buildings.

Table 2
Energy Saving Per Person (kWh/Person) During Summertime in the Photovoltaic Panel Cases in Absolute Values and in Percentage (in Brackets) With Respect to the Air Conditioning Systems Consumption

λ_p				
H	0.25	0.33	0.50	0.66
5 m ()	− 2.78 (−211%)	− 2.77 (−212%)	− 2.77 (−213%)	− 2.76 (−218%)
10 m ()	− 0.23 (−107%)	− 1.38 (−109%)	− 1.38 (−113%)	− 1.37 (− 119%)
20 m ()	− 0.69 (−53%)	− 0.68 (−55%)	− 0.68 (−60%)	− 0.67 (−67%)

energy with respect to consumption (if the ACSs energy saving in Table 2 is less than −100%, the production overcomes the demand). In the worst-case scenario ($H = 20$ m, $\lambda_p = 0.25$), the production of electricity allows a decrease of EC due to ACSs of ∼53% (−0.69 kWh per person on average), while, for $H = 5$ m and $\lambda_p = 0.66$, the consumption due to ACSs is less than half of the total energy produced by PVPs (2.78 kWh per person on average), under the assumption that the roof surface is totally covered by PVPs.

4.1.3. Temperatures and Energy Budget at the Roof Level

Figures 10 and 11 show the diurnal cycles of air and roof temperatures and of surface fluxes, respectively, for a roof situated in the center of the city, for all the simulations in the configuration with $H = 10$ m and $\lambda_p = 0.50$. This configuration has been chosen as an example to highlight the effects of the RMSs on the surface energy budget and on air and roof temperatures. Considering NORMS, the surface temperature reaches its maximum value (∼50°C) around noon, with a corresponding maximum in the outgoing sensible heat flux of ∼300 W m^{-2}. On the other hand, the peak of the internal roof layer temperature is reached at 17:00 LST (∼36°C), due to the thermal inertia of building materials. During nighttime surface roof temperature is always lower than the temperature of the internal layer, reaching a minimum value of ∼22°C at 04:00 LST.

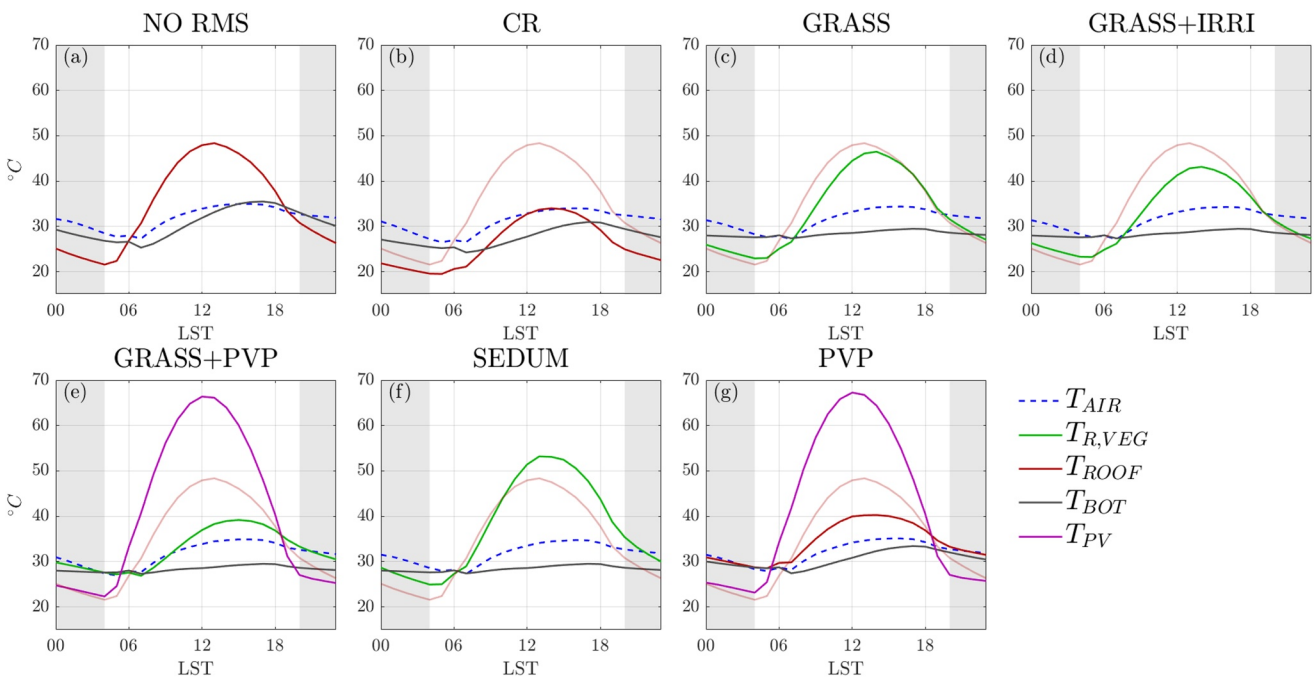

Figure 10. Summertime temperature diurnal cycles of first air layer above the roof (dashed blue), vegetated roof surface (green), upper roof layer (red), lower roof layer (gray), and PVP (purple), for the central cell representing the city, for the configuration with $H = 10$ and $\lambda_p = 0.50$. The temperature of the upper roof layer of NORMS is represented in pink also in the other panels for comparison. Shaded background indicates nighttime hours.

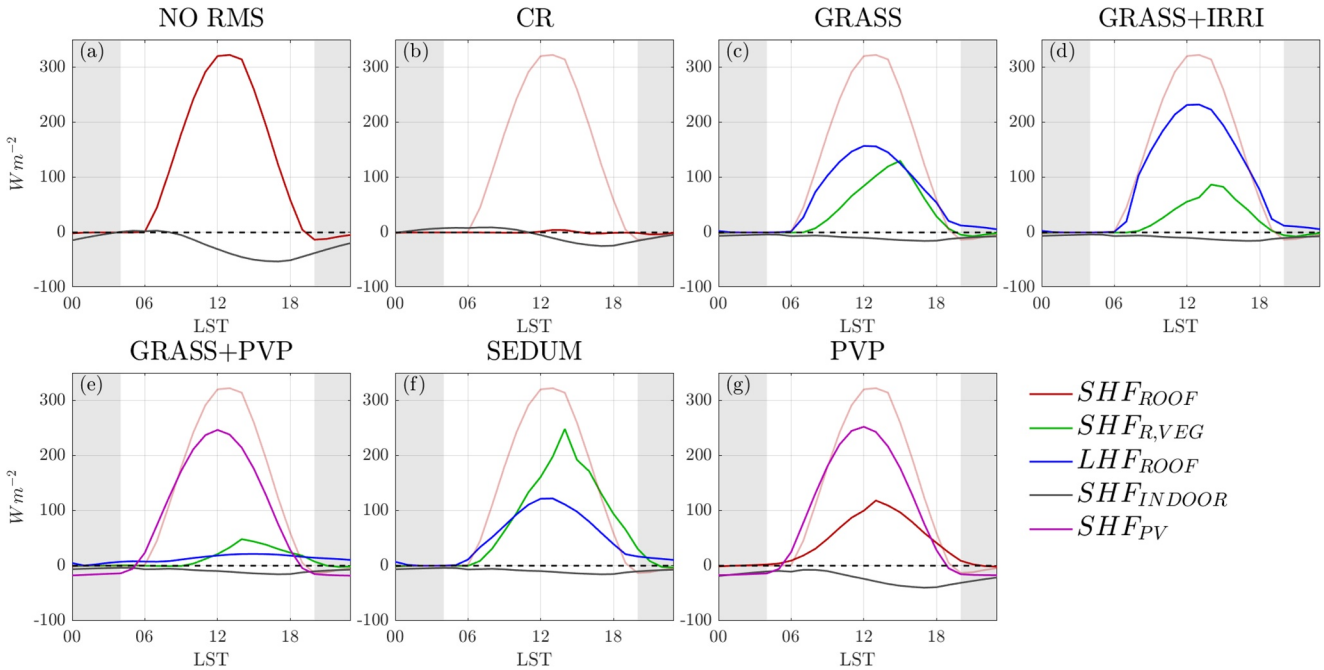

Figure 11. Summertime diurnal cycles of sensible heat flux for clay tiles roof (red), vegetated roof (green), indoor (gray), PVP (purple), and of latent heat flux for vegetation (blue), for the central cell representing the city, for the configuration with $H = 10$ and $\lambda_p = 0.50$. The sensible heat flux of NORMS is represented in pink also in the other panels for comparison. Shaded background indicates nighttime hours.

CRs have a significant impact on surface temperature, with maximum values reaching ~34°C, that is, 16°C less than NORMS, influencing also near-surface air temperature. Also the temperature of the internal roof layer is diminished by 4°C, causing the decrease of EC. In this case, the sensible heat flux is almost null during all the daily cycle. Regarding the scenarios implementing GRs, it is clear that the emission of latent heat flux from vegetation and natural soil is the principal factor in diminishing air temperature. Looking at GRASS, the maximum temperature of vegetation is slightly lower with respect to the clay tiles roof temperature by ~3°C, especially in the first part of the day. Moreover, the latent heat flux always overcomes the sensible heat flux. The peak of latent heat flux occurs at noon, two hours before the peak of sensible heat flux: this means that the impact of vegetation is more marked in the earlier hours of the day, resulting in a higher difference with respect to clay tiles roofs at noon, when also 2-m air temperature differences are larger, as shown in Figure 6. Also the temperature of the internal roof layer is lower (~5°C) with respect to NORMS: in this case, the waterproof insulating layers of the green roof prevent the heat to diffuse through building materials, and hence inside building rooms. This is evident also observing the indoor sensible heat flux, which is almost null for all the cases with GRs. Differences in magnitude between sensible and latent heat flux are even larger in GRASS + IRRI, since irrigation contributes to increase the soil moisture of the GR, and hence to increase the latent heat flux. On the other hand, since sedum is less efficient in converting solar radiation into latent heat flux with respect to grass, the roof temperature in SEDUM is similar before noon, and higher in the afternoon with respect to NORMS, probably because of the reduced diffusion of heat toward the internal layers of the roof, due to the waterproof insulating layers, that makes the substrate temperature higher. However, the temperature of the internal roof layer in SEDUM is comparable to the one in GRASS, strengthening the hypothesis that processes taking place within the building are not significantly affected by the vegetation type, but rather by the thermal properties of building materials.

Focusing on the PVP case, the panel temperature reaches very high maximum values (~67°C), corresponding to the peak of solar radiation. Despite a considerably higher temperature with respect to the environment, the outgoing heat flux from the PVP is lower with respect to the one from the clay tiles roof surface, because the material constituting the PVP is less efficient in releasing heat. However, the sum of the sensible heat flux from the PVP and the roof is higher than the sensible heat flux in NORMS. This explains why the temperature, especially in the first hours of the day, is higher with respect to NORMS. Moreover, the

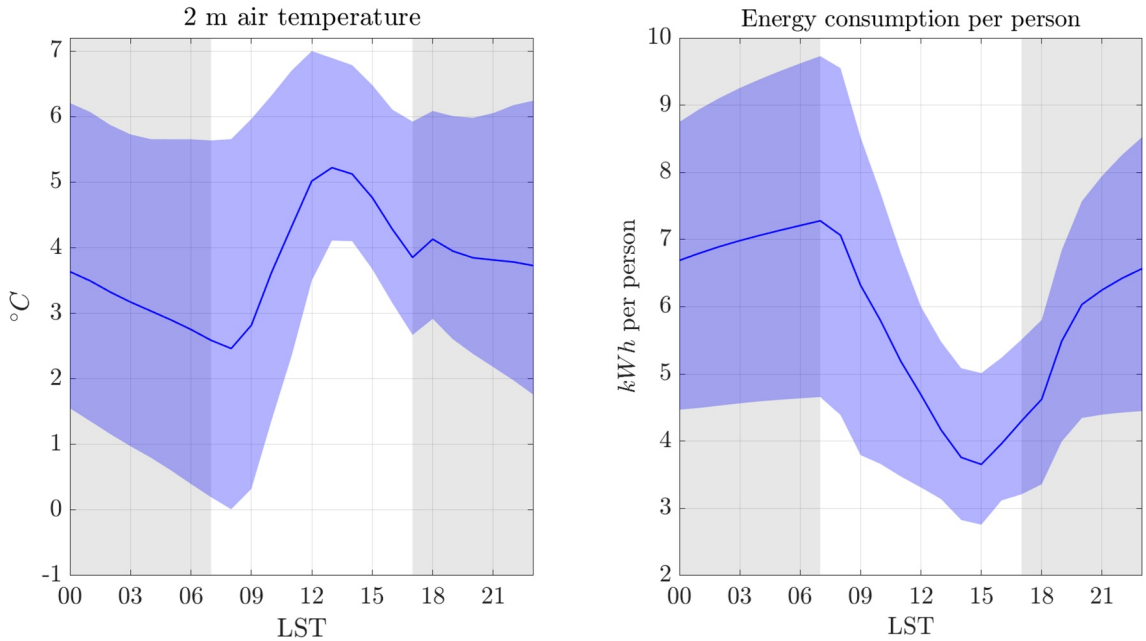

Figure 12. Wintertime average air temperature at 2-m AGL (left) and energy consumption per person (right) averaged over a single diurnal cycle for the NORMS simulations (blue line). The blue shaded regions represent the variability obtained in the simulations with different urban configurations. Shaded background indicates nighttime hours.

shading effect exerted by the PVP on the roof, despite the longwave radiation exchange between the two surfaces, decreases the surface temperature of the roof by ~8 °C, resulting in a lower EC due to ACSs during daytime. This has been observed even in the experimental study by Dominguez et al. (2011). On the other hand, during nighttime, PVP temperature is lower than both air and roof temperature, resulting in a negative heat flux (i.e., heat goes from the environment to the PVP), contributing to decreasing air temperature during nighttime. However, the screening effect of the PVP makes the roof warmer than the exposed roof of ~7°C, explaining the increase in EC shown by PVP during nighttime. Similar results, from an experimental campaign, are presented in Broadbent et al. (2019), where the temperature of the PVP is ~30°C higher during daytime and ~10°C lower during nighttime with respect to the one of the underlying surface.

No substantial differences with respect to PVP are shown by GRASS + PVP, in terms of temperature and fluxes of the PV module; this means that the heat exchange processes of the PVP are not significantly influenced by the characteristics of the underlying surface. On the other hand, shading affects the heat exchange between vegetation and the atmosphere: vegetation temperature in GRASS + PVP is slightly lower during daytime than in GRASS, because of the lower radiation that reaches the vegetation. Moreover, the sensible heat flux from vegetation is lower than the flux from a normal roof shaded by the PV, explaining why the diurnal temperature in GRASS + PVP is lower than the simple PVP case.

4.2. Wintertime

Figure 12 shows the diurnal cycle of 2-m air temperature (left) and EC per person due to space heating (right) during wintertime for the central cell representing the idealized city in the NORMS simulations. On average, the maximum temperature reached by the simulations is ~6°C at 13:00 LST, while the minimum value is ~3°C at 08:00 LST, depicting, as expected, a lower diurnal variability than the summer scenario. Temperature variability between different urban configurations is again larger during nighttime, due to the dependence of the UHI effect on urban geometry, with a range of ~5°C between the different urban configurations. The trend of the heating EC with time is opposite with respect to the summer case: EC is minimum during the central hours of the day, when solar radiation warms building materials, while it increases during nighttime, keeping a quasi-constant value from 00:00 to 06:00 LST. Also in this case EC variability between different urban configurations is higher with respect to temperature variability. Values

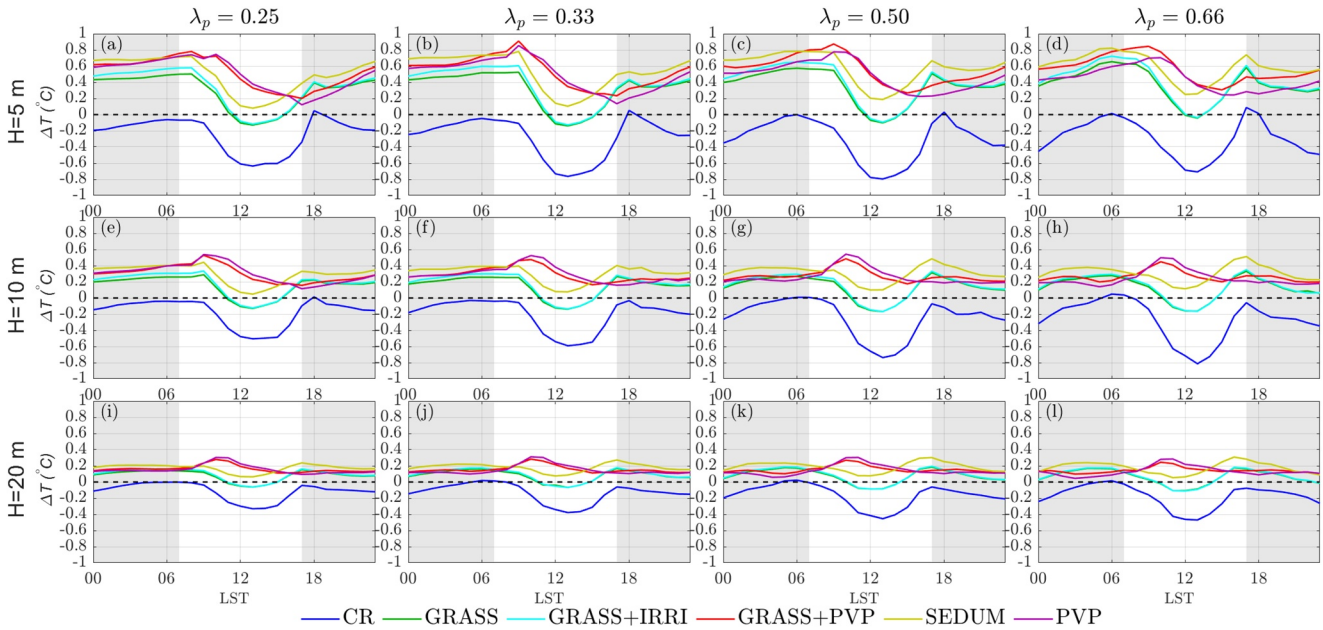

Figure 13.. Wintertime 2-m air temperature differences between NORMS and each rooftop mitigation strategy, averaged for the central urban cell, and for a single diurnal cycle. Building height is kept constant along the rows, while λ_p along the columns. Shaded background indicates nighttime hours.

are ~3 times higher with respect to the summer case; in fact, while the coefficient of performance (COP) for cooling systems is 3.5, for heating systems is 0.9, resulting in higher consumptions during wintertime and moreover temperature differences between the indoor air and the outside are larger.

4.2.1. Impact on 2-m Air Temperature

Figure 13 shows the time series of 2-m air temperature differences between NORMS and all the RMSs for all the possible urban configurations. It is worth noting that, opposite to the summer season, during wintertime a higher temperature is beneficial both for thermal comfort and for reducing EC due to heating. Figure 13 shows that, differently from the summer season (Figure 6), only CR decreases 2-m air temperature in winter. In general, the temperature in the simulations implementing GRs and PVPs is higher than in NORMS, especially during nighttime. The peak of temperature decrease for CR coincides with the peak of solar radiation, while the peak of increase for PVP takes place at 09:00 LST, at the same time as in the summer simulations. For all the RMSs and all the urban configurations, the differences with respect to NORMS are smaller than in the summer case: being winter solar radiation considerably weaker than during summertime, also the modifications of the surface energy budget induced by the RMSs are less significant in winter than in summer. Also in this case the highest differences with respect to NORMS occur in urban configurations with higher λ_p and lower buildings. In general, simulations with PVPs exhibit the highest temperature peaks, with an increase in 2-m air temperature up to ~0.9°C. This is again due to the instant release of heat by the panels, since they are much thinner than the roof and they respond quicker to solar radiation. On the other hand, during nighttime simulations with PVPs maintain a higher temperature than NORMS. PVPs act (a) avoiding radiation to be stored in the roof layers and (b) screening the roof, inhibiting the release of longwave radiation. Apparently, effect (b) is dominant in the winter case, since roof layers are now heated by the internal rooms. For this reason, PVPs prevent the heat produced by the heating systems to be released (Figure 17 shows that the nighttime temperature of the roof is ~5°C higher than the exposed roof), resulting in an increased air temperature during nighttime. The diurnal cycle of 2-m air temperature differences for CR is similar to the summer case, with the highest negative difference at noon (~−0.6°C for most cases). On the other hand, during nighttime CR maintains a temperature ~0.4°C lower than NORMS, and differences become null at sunrise. Simulations implementing GRs present the highest dissimilarities compared to the summer case: while during the central hours of the day (when thermal comfort is higher than at nighttime) 2-m air temperature differences with NORMS are often negative (~−0.2°C for all the configurations with $\lambda_p = 0.66$), in the evening and during nighttime

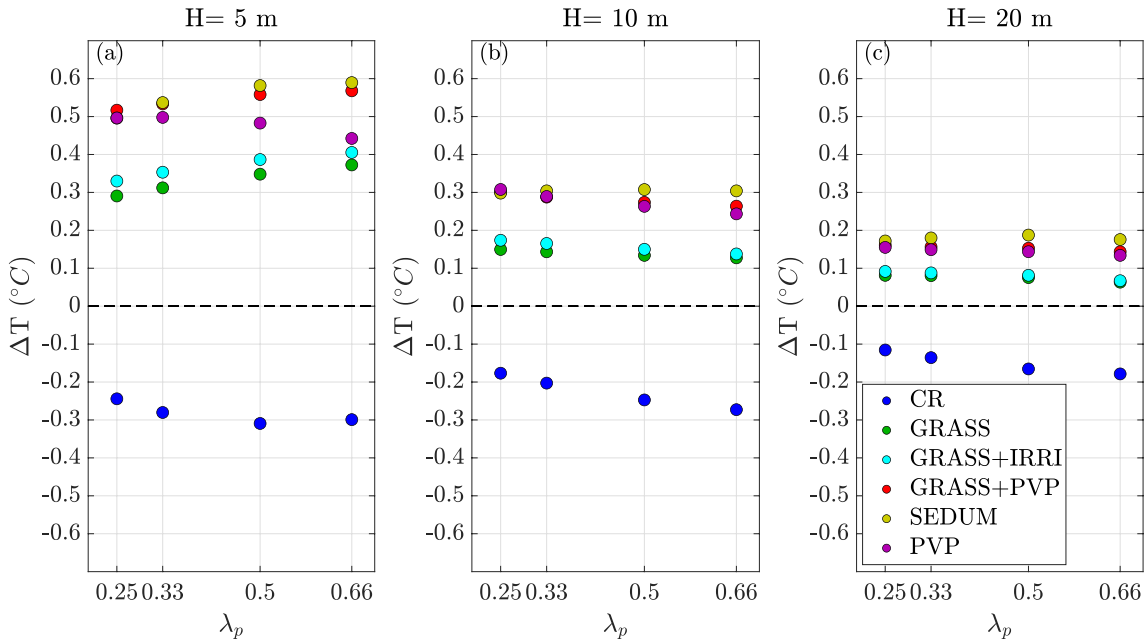

Figure 14. Wintertime 2-m air temperature differences for each rooftop mitigation strategy averaged over all the period of simulations, depending on λ_p. The left panel shows 5-m building configurations, the central panel 10-m buildings, and the right panel 20-m buildings.

all simulations with GRs show a higher temperature than NORMS, up to ~0.8°C for SEDUM. The increase in temperature, which is beneficial for both thermal comfort and EC, is mainly due to the combination of the higher thermal capacity of the GR with respect to the clay tiles roof (heat stored during daytime, and released in higher amounts during nighttime) and to the low latent heat flux during daytime (the low winter radiation never makes the latent heat flux to overcome the sensible heat flux, as shown in Figure 18). This is due to the fact that the stomatal resistance is inversely proportional to the solar radiation, and consequently the conversion of solar radiation into latent heat is less favored during wintertime. The effect of the reduced latent heat is clear if we refer to SEDUM: sedum vegetation is less efficient in converting solar radiation into latent heat flux, therefore this RMS is the one that shows the highest temperature differences with respect to NORMS. Finally, GRASS + PVP behaves similarly to PVP, with slight nighttime increases, due to the screening effect of the PVPs.

On average (Figure 14), 2-m temperature differences induced by the RMSs slightly increase with increasing λ_p for the $H = 5$ m cases (with the exception of PVP, which remains almost constant). The other building heights, apart from CR, whose average negative temperature differences becomes slightly larger with λ_p, show instead a constant increase in temperature at the different values of λ_p explored. SEDUM and GRASS + PVP are the RMSs showing the largest increases in temperature, and thus the largest benefits in terms of thermal comfort, up to ~0.6°C for the configuration with $\lambda_p = 0.66$ and $H = 5$ m. PVPs increases are comparable to the ones of SEDUM, but discrepancies are notable with increasing λ_p. It can also be observed that the positive differences (cases with GRs and PVPs) decrease faster increasing the building height than the negative differences induced by CRs.

4.2.2. Impact on Energy Consumption

Figure 15 shows the time series of the differences in EC per person due to space heating between NORMS and all the RMSs for all the urban configurations. Since EC is low during daytime, the effect of the RMSs takes place mainly during nighttime hours. During the night, at constant H (i.e., for each row of Figure 15) the differences in EC induced by the variation of λ_p are very low, due to fact that temperature differences are not influenced by this parameter (cf. Figure 14). The influence of GRs on EC does not depend on the type of vegetation and on soil moisture, since all the simulations with GRs show the same trend. In particular, while during daytime the differences with NORMS are small, from 00:00 to 11:00 LST all simulations with GRs depict a constant decrease in EC, up to 3 kWh per person for the $H = 5$ m cases, where the effect is

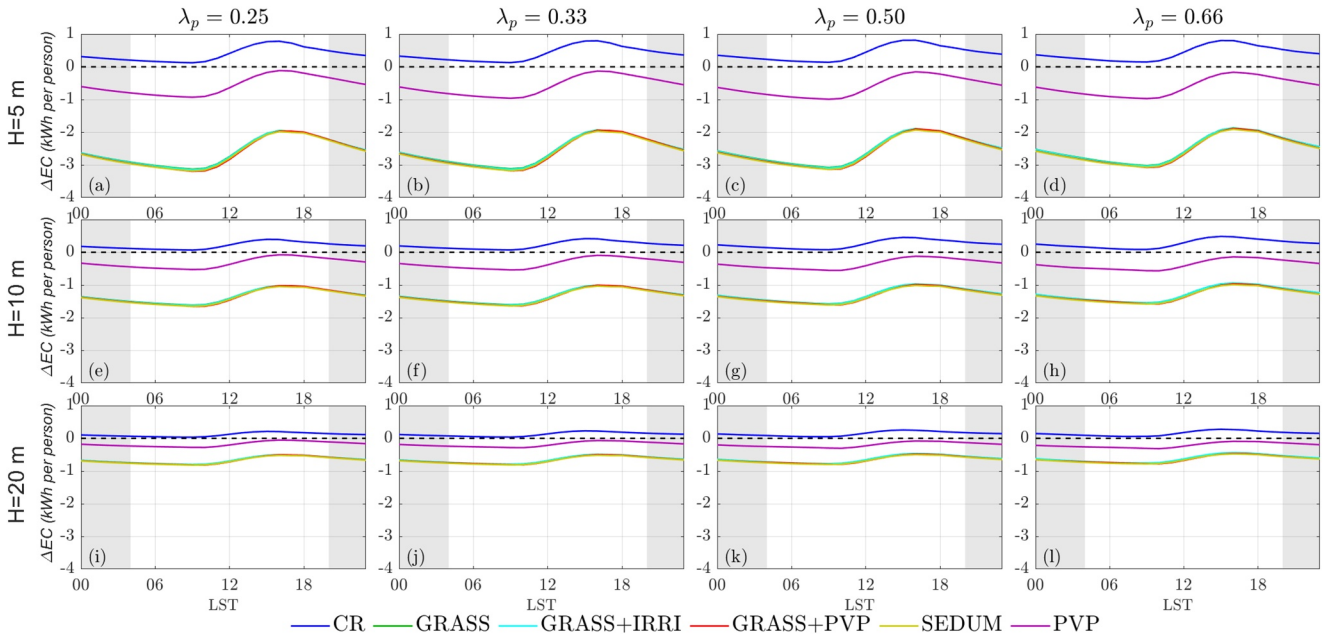

Figure 15. Differences in energy consumption per person between NORMS and each rooftop mitigation strategy averaged for the central urban cell and for a single diurnal cycle during wintertime. Building height is kept constant along the rows, while λ_p along the columns. Shaded background indicates nighttime hours (Notice that the range of the axes is different varying the building height).

stronger since buildings are composed of a single floor. Concerning CR, there is always an increase in EC by heating, especially for low buildings. Differences are almost null or slightly positive during nighttime, when the modified roof albedo does not affect the energy budget of the roof surface, while they display a maximum around 16:00 LST, due to the reduction of the roof surface temperature. PVPs present small differences with respect to NORMS in the afternoon and in the evening, while during night hours and in the morning the decrease in EC is more significant: while during daytime PVPs reduce roof surface temperature, during nighttime they trap the infrared radiation emitted by the roof, keeping it warmer than in NORMS and consequently decreasing the energy demand (see Figure 17).

Figure 16 shows the cumulative differences in the percentage of EC by heating per person between all RMSs and NORMS for all the simulations. As shown above, for the same building height, differences are almost insensitive to λ_p. Therefore, contrary to the summer case, street width does not influence the effects of RMSs on EC. Regarding PVP, differences are always negative as explained in the previous subsection (~8% for the $H = 5$ m cases), because of the screening effect on longwave radiation during the night. On the other hand, CR always increases EC by ~5% for all the urban configurations. Again, all the simulations with GRs show a relevant saving of EC by heating. In particular, the combined effect of insulation by waterproof layers and higher thermal capacity consents a reduction of the heating EC up to ~33% for the $H = 5$ m cases, and of ~22% and ~15% for the $H = 10$ m and $H = 20$ m cases, respectively. As in the summer case, there are no relevant differences induced by the GR vegetation type and the soil moisture availability, indicating that the insulating layers are the dominating effect in reducing EC by heating.

In Table 3, the energy saving per person in the PVP simulations, in percentage with respect to the heating consumption and on average over the period of integration, is shown, assuming to instantly use the energy produced by the photovoltaic modules for heating: in contrast to the summer case, during wintertime electricity production never overcomes energy demand, due to the fact that the energy produced by PVPs is lower than during summertime, due to the lower incoming solar radiation. The maximum reduction is 0.67 kWh per person, compared to 2.78 kWh per person in the summer period, that is, roughly four times lower. In particular, the maximum percentage saving of ~ 15% is reached for the $H = 5$ m cases, while for 20-m tall buildings, heating EC can be reduced by up to 13%.

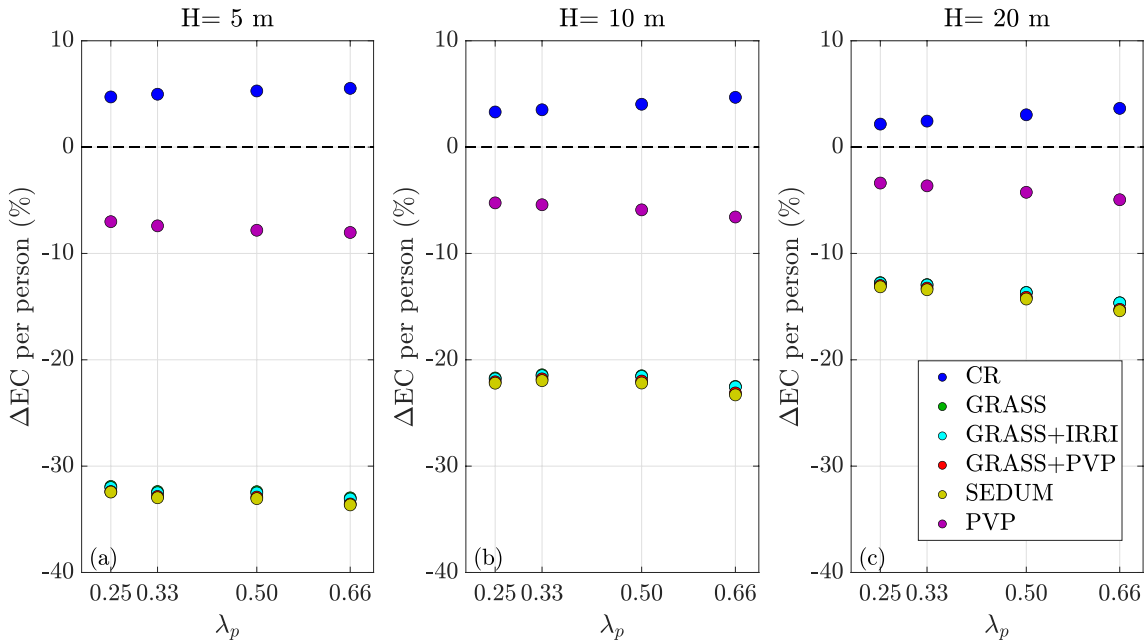

Figure 16. Variation (percentage) in energy consumption per person with respect to the NORMS case, for each rooftop mitigation strategy for all the period of simulation during wintertime, depending on λ_p. The left panel shows results for 5-m buildings, the central panel for 10-m buildings and the right panel for 20-m buildings.

4.2.3. Temperatures and Energy Budget at the Roof Level

Figures 17 and 18 show the time series of air and roof temperature and of heat fluxes, respectively, for the configuration with $\lambda_p = 0.50$ and $H = 10$ m for the winter season, for all the simulations. Considering NORMS, as in the summer season, roof temperature is higher than air temperature during daytime and lower during nighttime, reaching a maximum temperature of ~10°C at 13:00 LST and a minimum value of ~0°C after sunset. Contrarily to the summer case, the temperature of the internal roof layer is always higher than both air and roof surface temperature, since a target temperature of 20°C is required for the building rooms. The temperature of the internal roof layer oscillates between ~10°C during nighttime and ~15°C during daytime, always lower than the target temperature. Since the temperature of the internal roof layer is always higher than the external surface temperature, the indoor heat flux is always outgoing (i.e., from the internal room to the environment), with minimum values during daytime, when solar radiation heats the roof. CR behaves as in the summer case: roof temperature is reduced, comparable with the NORMS roof during nighttime and with air temperature during daytime. Internal roof temperature is lower than NORMS, especially during daytime. During daytime PVP acts similarly to CR: the PVP prevents the radiation to reach the roof surface, thus the roof is cooler than in NORMS, despite the PVP temperature reaches ~15°C. On the other hand, during nighttime, the roof, shielded by the PVP, is warmer (~5°C) than in NORMS. PVP temperature during nighttime is much lower than the air temperature, with differences of ~6°C, with a resulting negative PVP sensible heat flux (~−30 W m^{-2}). The heat flux from the roof covered by

Table 3
Energy Saving Per Person (kWh/Person) During Wintertime in the Photovoltaic Panels Cases in Absolute Values and in Percentage (in Brackets) With Respect to the Heating Consumption

λ_p				
H	0.25	0.33	0.50	0.66
5 m	− 0.67 (−13%)	− 0.68 (−14%)	− 0.69 (−14%)	− 0.70 (−15%)
10	− 0.36 (−9%)	− 0.37 (−9%)	− 0.38 (−10%)	− 0.39 (− 11%)
20 m	− 0.19 (−6%)	− 0.19 (−6%)	− 0.20 (−7%)	− 0.20 (−8%)

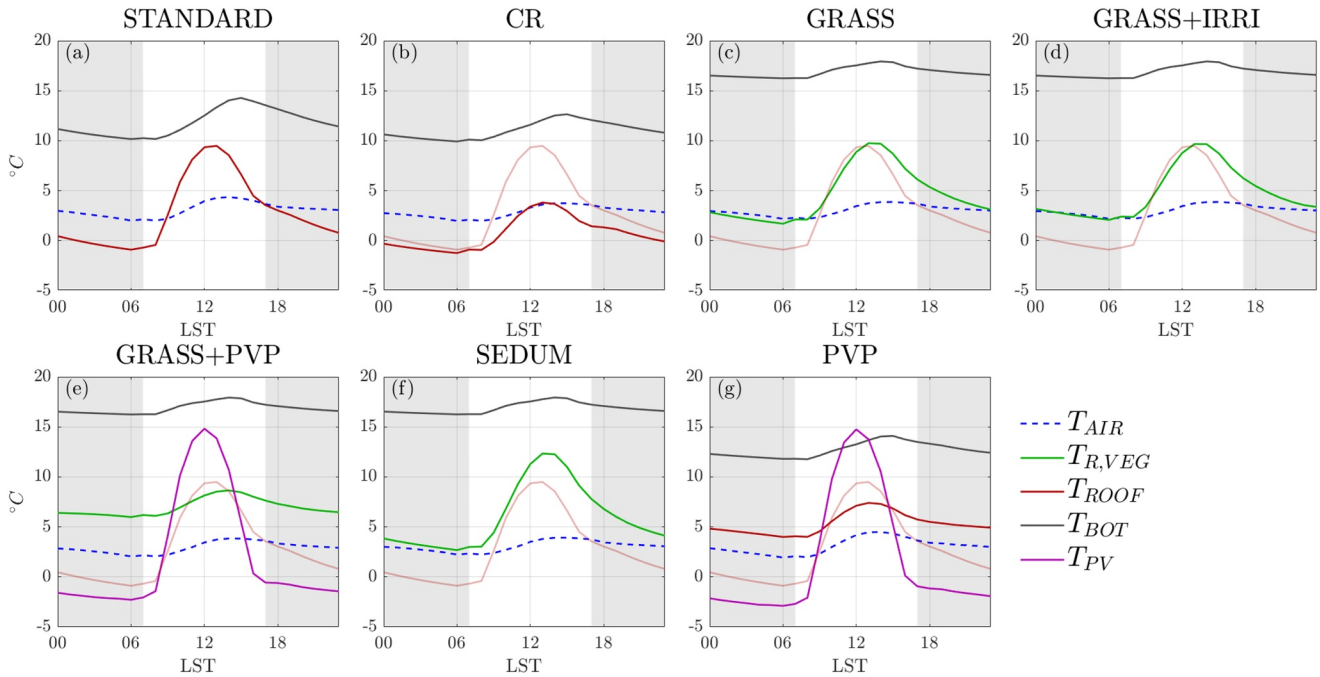

Figure 17. Wintertime diurnal cycle of temperature of near-surface air (dashed blue), vegetated roof (green), upper roof layer (red), lower roof layer (gray), and photovoltaic panel (PVP, purple), for the central cell representing the city, for the $H = 10$ m, $\lambda_p = 0.50$ configuration. The temperature of the upper roof layer of NORMS is represented in pink also in the other panels for comparison. Shaded background indicates nighttime hours.

the PVP remains significantly positive even during nighttime, explaining the higher air temperature in PVP simulations during night hours. Simulations with GRs instead show an increase of roof surface temperature with respect to NORMS, especially after 13:00 LST and during nighttime. In this time period GRs are

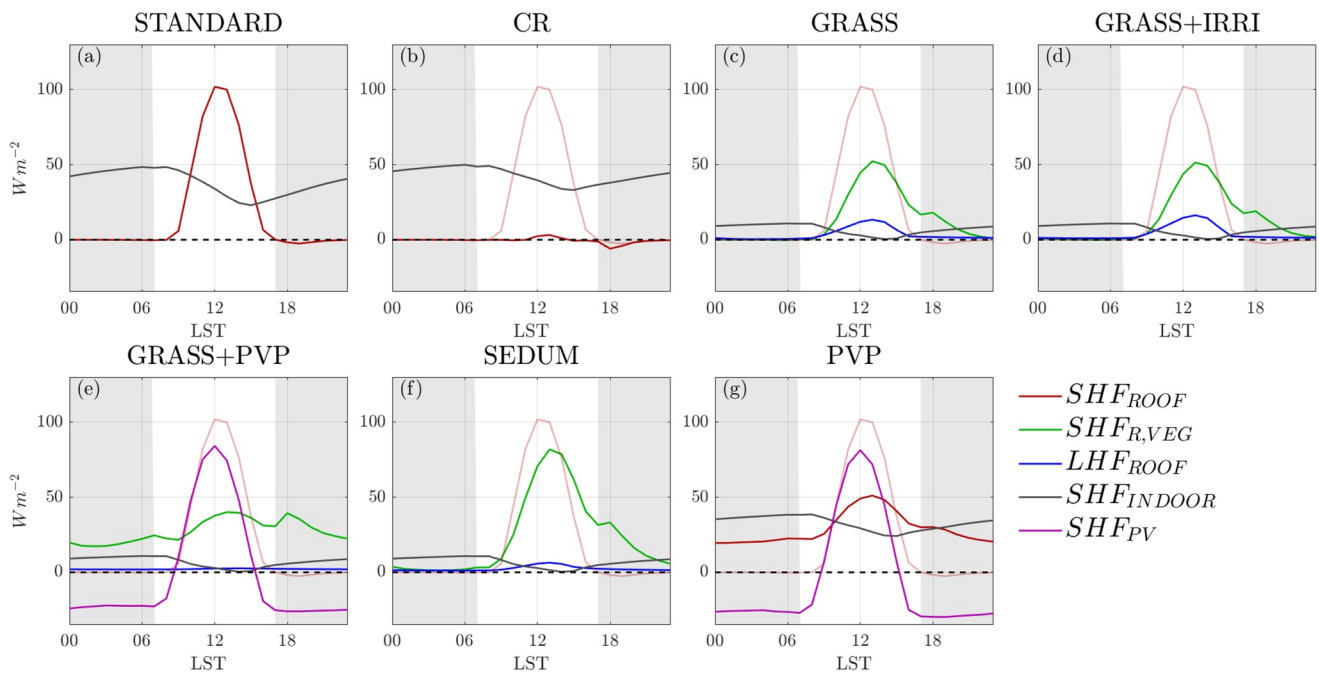

Figure 18. Wintertime diurnal cycle of sensible heat flux for clay tiles roof (red), vegetated roof (green), indoor (gray), photovoltaic panel (PVP, purple), and of latent heat flux for vegetation (blue), for the central cell representing the city, for the $H = 10$ m, $\lambda_p = 0.50$ configuration. The sensible heat flux of NORMS is represented in pink also in the other panels for comparison. Shaded background indicates nighttime hours.

warmer than NORMS by ~5°C due to the combination of (a) the reduced upward latent heat flux (almost null even during daytime), due to a lower incoming shortwave radiation in the winter season with respect to summertime and (b) the higher volumetric thermal capacity of the GR layers with respect to the clay tiles roof, resulting in a reduction of the upward sensible heat flux during daytime, and an increase during nighttime. In fact, while the peak of the upward sensible heat flux in NORMS is ~100 W m^{-2}, the peak in the simulations with GRs is ~50 W m^{-2} and shifted in time, due to the higher thermal inertia. Moreover, just after sunset, the upward sensible heat flux assumes slightly positive values, increasing outdoor temperature, as seen in Section 4.2.1. The effect of insulating waterproof layers is again clear looking at the temperature of the internal roof layer, which is constantly warmer than in NORMS by ~7°C, and from the indoor sensible heat flux, that oscillates around zero. Regarding SEDUM, the lower efficiency in converting radiation into latent heat flux with respect to grass is beneficial during wintertime, since roof surface temperature is higher than in GRASS, and contributes to increasing air temperature. Finally, GRASS + PVP behaves similar to PVP, with an almost null latent heat flux during all the day, and nocturnal sensible heat flux higher than in the PVP case, resulting in higher temperatures than in PVP during nighttime.

5. Discussion and Conclusions

This study presented the results of two-dimensional idealized simulations with the mesoscale WRF model in the urban environment, implementing innovative parameterizations of RMSs, coupled with the BEP-BEM urban parameterization schemes. In particular, simulations were performed under two different climatic conditions (i.e., summertime and wintertime), for 12 different urban configurations, with the aim of quantifying the effect of different RMSs, that is, cool roofs, green roofs, and rooftop photovoltaic panels, on 2-m air temperature and on EC, for several urban geometries. Below we summarize the key results, highlighting the main differences between simulations implementing rooftop mitigation strategies and a simulation with clay tiles roofs, taken as the reference:

1. Dependence of air temperature on urban configuration

The mitigation effect on air temperature varies almost linearly with the building surface to total surface fraction (λ_p) during summertime, while in wintertime it linearly increases only for 5-m high buildings. The mitigation effect is higher for low buildings, with a nonlinear decrease of the impact with building height. Therefore, the urban configuration with the lowest buildings and the highest λ_p ($H = 5$ m and $\lambda_p = 0.66$) shows the highest effect of the RMSs.

2. Dependence of energy consumption on urban configuration

During summertime, similarly to temperature, the saving of EC per person by ACSs induced by RMSs increases linearly with λ_p, and decreases with building height, since RMSs act mostly on the floor just below the roof. During wintertime, instead, no dependence of EC by heating with varying λ_p was detected. As in the summer case, the energy saving percentage decreases as the building height increases.

3. Temperature mitigation during summertime

All mitigation strategies with CRs and GRs induce a decrease in air temperature with respect to the clay tiles roof, with a greater effect during daytime. For these RMSs, the highest temperature reductions occur starting from the central daytime hours, with a secondary peak before sunrise. In general, CR is the most efficient in reducing summer temperatures, with a maximum decrease of ~3.3°C and a daily average decrease of ~2.2°C for the urban configuration with $H = 5$ m and $\lambda_p = 0.66$. The second most efficient RMS is GRASS + IRRI, thanks to the latent heat flux increased by irrigation. SEDUM is the RMS employing GRs with the smallest impact on air temperature: sedum vegetation is less efficient in converting solar radiation into latent heat flux, hence the mitigation effect is, in general, less than half with respect to GRASS. Air temperature in PVPs increase during daytime because the heat flux from PVPs is instantly released and

summed to the heat flux from the roof surface. On the other side, during nighttime PVP maintains a lower temperature until sunrise, due to the reduction of the heat stored within the building materials during daytime. On average, PVPs slightly decrease thermal comfort. This result is in contrast with the works of Masson et al. (2014) and Salamanca et al. (2016), but it is consistent with different observational data that demonstrate that PVPs generally increase temperature during daytime (Barron-Gafford et al., 2016; Broadbent et al., 2019). Results of GRASS + PVP are mainly driven by the PVP energy balance, with higher reductions with respect to PVP, both during daytime and nighttime, due to the GRs presence.

4. Energy consumption during summertime

In general, CRs and GRs decrease EC by ACSs, with the maximum saving during the late afternoon. All simulations implementing GRs, even the one with overlaying PVPs, show the same behavior, since for EC the dominant feature is the insulating effect of the waterproof layers constituting the GR (and not the vegetation type), and they are the most efficient during daytime. The effect of CRs is comparable to that of GRs during daytime, while during nighttime hours the reduction in EC is larger than in the GR cases, because the increased albedo decreases the heat storage within the roof. On average, CR can save up to 45% of EC by ACs (for the urban configuration with $H = 5$ m and $\lambda_p = 0.66$), while the average effect of PVPs is null. If we assume to employ all the electricity produced by PVPs for the ACSs supply, we obtain a net gain for all the urban configurations, with an energy production up to ~210% of the ACSs EC for 5-m buildings.

5. Temperature mitigation during wintertime

Contrary to summertime, during wintertime RMSs are beneficial if they induce an increase in air temperature. During wintertime, CRs act similarly to the summer period, i.e., diminishing temperature during all the day, with higher reductions during daytime, corresponding to the peak of solar radiation. However, since during wintertime solar radiation forcing is weaker, the reduction is limited to up to ~0.3°C, around 10 times less than in summertime. On the other hand, all simulations with GRs perform differently with respect to summertime. Since the latent heat flux is greatly reduced, because of the dependence of stomatal resistance on solar radiation, more energy is stored in building materials. As a consequence, more heat is released during nighttime: since sedum vegetation is the less efficient in triggering evapotranspiration, SEDUM is the most efficient in warming up during wintertime, with an average increase of ~0.5°C for the configuration with $H = 5$ m and $\lambda_p = 0.66$. Even PVPs increase 2-m air temperature during the winter season: during daytime the effect is the same as in the summer case, while during nighttime they prevent the roof cooling by longwave radiation release, with a consequent higher temperature up to ~0.8°C.

6. Energy consumption during wintertime

The temperature decrease induced by CRs during wintertime causes an increase in EC by heating of ~5% for all the urban configurations. On the other hand, PVP slightly decreases the energy demand (around ~6%), because of the combined effect of the temperature increase and the screening of the PVP for longwave radiation during nighttime. The electricity produced by PVPs is not sufficient to cover all the EC by heating, due to the lower energy production from the weak incoming solar radiation. All the simulations with GRs, because of the combined effect of increased external temperatures and of the insulating layer (that prevents the diffusion of indoor heat through the roof), reduce EC up to 35% for the urban configurations with $H = 5$ m.

The aim of this study was to quantify the effect of various rooftop mitigation technologies under different climatic conditions, in order to set a benchmark for urban climate studies. A wide range of urban configurations with uniform building heights, under two typical climate scenarios was investigated, so as to provide a comprehensive set of results, that can be representative of most midlatitude cities. Results, limited to simplified urban geometrical configurations, pointed out that advanced parameterization schemes are needed to simulate the complex feedback between buildings and the atmosphere, in order to obtain reliable results, that can be used by urban planners and decision-makers to make informed choices to improve the sustainability of urban areas.

Data Availability Statement

The model is currently implemented in the new WRF version (4.3.1): https://github.com/wrf-model/WRF.git. Simulations output can be found at https://github.com/andreazonato/RMS_IDEALIZED_SIMULATIONS.git.

Acknowledgments
The authors would like to acknowledge high-performance computing support from Cheyenne (https://doi.org/10.5065/D6RX99HX) provided by NCAR's Computational and Information Systems Laboratory, sponsored by the National Science Foundation and the Advance Study Program's Graduate Student (GVP) Fellowship for the financial support. Open Access Funding provided by Universita degli Studi di Trento within the CRUI-CARE Agreement.

References

Barron-Gafford, G., Minor, R., Allen, N., Cronin, A. D., Brooks, A. E., & Pavao-Zuckerman, M. A. (2016). The photovoltaic heat island effect: Larger solar power plants increase local temperatures. *Scientific Reports*, *6*, 35070. https://doi.org/10.1038/srep35070

Bougeault, P., & Lacarrere, P. (1989). Parameterization of orography-induced turbulence in a mesobeta-scale model. *Monthly Weather Review*, *1172*(8), 1872–1890. https://doi.org/10.1175/1520-0493(1989)117<1872:POOITI>2.0.CO;2

Broadbent, A. M., Krayenhoff, E. S., Georgescu, M., & Sailor, D. J. (2019). The observed effects of utility-scale photovoltaics on near-surface air temperature and energy balance. *Journal of Applied Meteorology and Climatology*, *58*(5), 989–1006. https://doi.org/10.1175/jamc-d-18-0271.1

Chapman, S., Watson, J. E. M., Salazar, A., Thatcher, M., & McAlpine, C. A. (2017). The impact of urbanization and climate change on urban temperatures: A systematic review. *Landscape Ecology*, *32*(10), 1921–1935. https://doi.org/10.1007/s10980-017-0561-4

De Munck, C., Lemonsu, A., Masson, V., Le Bras, J., & Bonhomme, M. (2018). Evaluating the impacts of greening scenarios on thermal comfort and energy and water consumptions for adapting Paris city to climate change. *Urban Climate*, *23*, 260–286. https://doi.org/10.1016/j.uclim.2017.01.003

De Munck, C., Pigeon, G., Masson, V., Meunier, F., Bousquet, P., Tréméac, B., et al. (2013). How much can air conditioning increase air temperatures for a city like Paris, France? *International Journal of Climatology*, *33*(1), 210–227. https://doi.org/10.1002/joc.3415

de Munck, C. S., Lemonsu, A., Bouzouidja, R., Masson, V., & Claverie, R. (2013). The GREENROOF module (v7.3) for modelling green roof hydrological and energetic performances within TEB. *Geoscientific Model Development*, *6*(6), 1941–1960. https://doi.org/10.5194/gmd-6-1941-2013

Dominguez, A., Kleissl, J., & Luvall, J. C. (2011). Effects of solar photovoltaic panels on roof heat transfer. *Solar Energy*, *85*(9), 2244–2255. https://doi.org/10.1016/j.solener.2011.06.010

Eurostat (2018). *Living conditions in Europe, 2018 edition*. https://doi.org/10.2785/39876

Giovannini, L., Zardi, D., de Franceschi, M., & Chen, F. (2014). Numerical simulations of boundary-layer processes and urban-induced alterations in an Alpine valley. *International Journal of Climatology*, *34*(4), 1111–1131. https://doi.org/10.1002/joc.3750

Grimmond, C. S. B., & Oke, T. R. (1999). Aerodynamic properties of urban areas derived from analysis of surface form. *Journal of Applied Meteorology*, *382*(9), 1262–1292. https://doi.org/10.1175/1520-0450(1999)038<1262:APOUAD>2.0.CO;2

Gutierrez, E. (2015). *Quantification of environmental impacts of heat fluxes from built environments* (Unpublished doctoral dissertation). The City University of New York.

Jacquemin, B., & Noilhan, J. (1990). Sensitivity study and validation of a land surface parameterization using the HAPEX-MOBILHY data set. *Boundary-Layer Meteorology*, *52*(1–2), 93–134. https://doi.org/10.1007/BF00123180

Jones, A. D., & Underwood, C. P. (2002). A thermal model for photovoltaic systems. *Fuel and Energy Abstracts*, *43*(3), 199. https://doi.org/10.1016/S0140-6701(02)85831-3

Kolokotroni, M., Gowreesunker, B., & Giridharan, R. (2013). Cool roof technology in London: An experimental and modelling study. *Energy and Buildings*, *67*, 658–667. https://doi.org/10.1016/j.enbuild.2011.07.011

Kusaka, H., Kondo, H., Kikegawa, Y., & Kimura, F. (2001). A simple single-layer urban canopy model for atmospheric models: Comparison with multi-layer and slab models. *Boundary-Layer Meteorology*, *101*(3), 329–358. https://doi.org/10.1023/A:1019207923078

Lai, D., Liu, W., Gan, T., Liu, K., & Chen, Q. (2019). A review of mitigating strategies to improve the thermal environment and thermal comfort in urban outdoor spaces. *The Science of the Total Environment*, *661*, 337–353. https://doi.org/10.1016/j.scitotenv.2019.01.062

Li, D., & Bou-Zeid, E. (2013). Synergistic interactions between urban heat islands and heat waves: The impact in cities is larger than the sum of its parts. *Journal of Applied Meteorology and Climatology*, *52*(9), 2051–2064. https://doi.org/10.1175/jamc-d-13-02.1

Li, D., Bou-Zeid, E., & Oppenheimer, M. (2014). The effectiveness of cool and green roofs as urban heat island mitigation strategies. *Environmental Research Letters*, *9*(5), 055002. https://doi.org/10.1088/1748-9326/9/5/055002

Louis, J. F. (1979). A parametric model of vertical eddy fluxes in the atmosphere. *Boundary-Layer Meteorology*, *17*(2), 187–202. https://doi.org/10.1007/BF00117978

Martilli, A. (2014). An idealized study of city structure, urban climate, energy consumption, and air quality. *Urban Climate*, *10*(P2), 430–446. https://doi.org/10.1016/j.uclim.2014.03.003

Martilli, A., Clappier, A., & Rotach, M. W. (2002). An urban surface exchange parametrization for mesoscale models. *Boundary-Layer Meteorology*, *104*(2), 261–304. https://doi.org/10.1023/a:1016099921195

Masson, V. (2000). A physically-based scheme for the urban energy budget in atmospheric models. *Boundary-Layer Meteorology*, *94*(3), 357–397. https://doi.org/10.1023/a:1002463829265

Masson, V., Bonhomme, M., Salagnac, J. -L., Briottet, X., & Lemonsu, A. (2014). Solar panels reduce both global warming and urban heat island. *Frontiers in Environmental Science*, *2*, 1–10. https://doi.org/10.3389/fenvs.2014.00014

Mlawer, E. J., Taubman, S. J., Brown, P. D., Iacono, M. J., & Clough, S. A. (1997). Radiative transfer for inhomogeneous atmospheres: RRTM, a validated correlated-k model for the longwave. *Journal of Geophysical Research*, *102*(14), 16663–16682. https://doi.org/10.1029/97JD00237

Niu, G. Y., Yang, Z. L., Mitchell, K. E., Chen, F., Ek, M. B., Barlage, M., et al. (2011). The community Noah land surface model with multiparameterization options (Noah-MP): 1. Model description and evaluation with local-scale measurements. *Journal of Geophysical Research*, *116*, D12109. https://doi.org/10.1029/2010JD015139

NREL (2020). *Best research-cell efficiencies chart*. Retrieved From https://www.nrel.gov/pv/cell-efficiency.html

Oke, T. R., Mills, G., Christen, A., & Voogt, J. A. (2017). *Urban climates*. Cambridge, UK: Cambridge University Press. https://doi.org/10.1017/9781139016476

Pappaccogli, G., Giovannini, L., Cappelletti, F., & Zardi, D. (2018). Challenges in the application of a WRF/Urban-TRNSYS model chain for estimating the cooling demand of buildings: A case study in Bolzano (Italy). *Science and Technology for the Built Environment*, *24*(5), 529–544. https://doi.org/10.1080/23744731.2018.1447214

Pappaccogli, G., Giovannini, L., Zardi, D., & Martilli, A. (2020). Sensitivity analysis of urban microclimatic conditions and building energy consumption on urban parameters by means of idealized numerical simulations. *Urban Climate*, *34*, 100677. https://doi.org/10.1016/j.uclim.2020.100677

Salamanca, F., Georgescu, M., Mahalov, A., Moustaoui, M., & Martilli, A. (2016). Citywide impacts of cool roof and rooftop solar photovoltaic deployment on near-surface air temperature and cooling energy demand. *Boundary-Layer Meteorology*, *161*(1), 203–221. https://doi.org/10.1007/s10546-016-0160-y

Salamanca, F., Krpo, A., Martilli, A., & Clappier, A. (2010). A new building energy model coupled with an urban canopy parameterization for urban climate simulations-part I. formulation, verification, and sensitivity analysis of the model. *Theoretical and Applied Climatology*, *99*(3–4), 331–344. https://doi.org/10.1007/s00704-009-0142-9

Salamanca, F., Zhang, Y., Barlage, M., Chen, F., Mahalov, A., & Miao, S. (2018). Evaluation of the WRF-urban modeling system coupled to Noah and Noah-MP land surface models over a semiarid urban environment. *Journal of Geophysical Research: Atmospheres*, *123*, 2387–2408. https://doi.org/10.1002/2018JD028377

Santamouris, M. (2014). Cooling the cities—A review of reflective and green roof mitigation technologies to fight heat island and improve comfort in urban environments. *Solar Energy*, *103*, 682–703. https://doi.org/10.1016/j.solener.2012.07.003

Scherba, A., Sailor, D. J., Rosenstiel, T. N., & Wamser, C. C. (2011). Modeling impacts of roof reflectivity, integrated photovoltaic panels and green roof systems on sensible heat flux into the urban environment. *Building and Environment*, *46*(12), 2542–2551. https://doi.org/10.1016/j.buildenv.2011.06.012

Short, D., Dawes, R. W., & White, I. (1995). The practicability of using Richards' equation for general purpose soil-water dynamics models. *Environment International*, *21*(5), 723–730. https://doi.org/10.1016/0160-4120(95)00065-S

Skamarock, W., Klemp, J., Dudhia, J., Gill, D., Zhiquan, L., Berner, J., & Huang, X.-Y. (2019). *A description of the advanced research WRF model Version 4*. (NCAR Technical Note NCAR/TN-475+STR (p. 145). https://doi.org/10.5065/1dfh-6p97

Stamnes, K., Tsay, S. C., Wiscombe, W., & Jayaweera, K. (1988). Numerically stable algorithm for discrete-ordinate-method radiative transfer in multiple scattering and emitting layered media. *Applied Optics*, *27*(12), 2502–2509. https://doi.org/10.1364/ao.27.002502

UNI/TS 11300-1 (2014). *Energy performance of buildings. Part 1: Evaluation of energy need for space heating and cooling*. Rome: Italian Unification Institution.

US Department of Energy (2010). *EnergyPlus Engineering reference: The reference to EnergyPlus calculations* (p. 868). US Department of Energy.

Yang, L., Yan, H., & Lam, J. C. (2014). Thermal comfort and building energy consumption implications—A review. *Applied Energy*, *115*, 164–173. https://doi.org/10.1016/j.apenergy.2013.10.062

Zonato, A., Martilli, A., Di Sabatino, S., Zardi, D., & Giovannini, L. (2020). Evaluating the performance of a novel WUDAPT averaging technique to define urban morphology with mesoscale models. *Urban Climate*, *31*, 100584. https://doi.org/10.1016/j.uclim.2020.100584